

## Chapter 4

### **Proto-Kern Canyon Fault, the Northern Segment: A Structural Analysis**

#### **Introduction**

Steeply dipping strike-slip fault zones of Mesozoic age are common in the Sierra Nevada batholith (SNB). Many of these fault zones are the direct result of Farallon plate subduction beneath the western edge of North America. At ca. 100 Ma, the trajectory and rate of plate subduction changed from  $\sim$ N 40° E and 55 mm/yr to  $\sim$ N 30° E and 110 mm/yr (Engebretson et al., 1985). This change in plate trajectory and doubling of subduction rate are thought to have caused partitioning into the active magmatic arc of the dextral shear component of the obliquely directed Farallon plate subduction (Busby-Spera and Saleeby, 1990; Tikoff and Greene, 1994; Greene and Schweickert, 1995; Tobisch et al., 1995; Tikoff and Saint Blanquat, 1997).

Erosion and exhumation of the SNB has brought the roots of these ancient fault zones to the surface. These Mesozoic faults are better described as ductile shear zones, because deformation is widely distributed along rocks that deformed ductilely under high-temperature conditions. In ductile shear zones, it is likely that deformation initiates along weak zones, and with progressive deformation, the number of these zones increases and the zones merge into a wide region of broadly distributed shear, though other scenarios are also possible.

This chapter concentrates on one such ductile shear zone, the 130 km long Proto-Kern Canyon fault (PKCF), which was active between ca. 95–80 Ma. Along the northern

segment of the PKCF, depths of exposure are ~12–15 km (Chapter 3) and ductile deformation is preserved over a pervasively mylonitized, 2 km wide zone along the contact between ca. 90 Ma intrusive rocks and Mesozoic-age metamorphic pendant rocks. The presence of domainal shears outside of the main PKCF zone suggests that deformation was broadly distributed laterally over at least 5 km. Progressing southward along the southern SNB, the PKCF is exposed at progressively deeper levels. Along the southernmost segment of the PKCF, where depths of exhumation reach up to 26 km (Chapter 3), mylonitization is pervasive over a 5 km wide zone.

This study assesses the distribution of strain through different rock types along the mid- to upper-crustal level (~12 km) of the PKCF. The rocks deformed along the PKCF include 89 Ma granitic plutonic rocks, and Triassic-Jurassic marble, calcsilicate, micaceous quartzite, and phyllite. Studies of ductile straining and strain recovery mechanisms in analogous materials are compared to thin sections of rocks deformed along the PKCF. This analysis assigns the strain weakening regimes of Hirth and Tullis (1992) to rocks of the PKCF. In addition, an estimate of offset along the northern segment of the PKCF is made. The vertical distribution of slip in strike-slip fault zones is not well known, but models suggest that, although slip rate is fastest where the fault breaks the ground surface, the slip rate along deep faults (up to 15 km depth) actually increases with depth (Rolandone and Jaupart, 2002). At midcrustal levels, displacements can be significant on ductile shear zones, as deformation is distributed over broad zones and rocks deform internally as strain accumulates with time (Teyssier et al., 1991). In general within shear zones, the maximum finite stretch is sub-parallel with the fault zone, and along the transport direction. Although it is difficult to accurately measure

displacement within a ductile shear zone because offset markers are typically vague, rock fabrics arising from internal straining and thinning of material within the main deformation zone may be used to estimate offset (Ramsay and Graham, 1970; Mitra, 1979). This method is applied to estimate offset on the PKCF, and combined with strain studies, indicates significant deformation and offset over a broadly distributed zone of heterogeneous shear.

## **Geologic Setting**

### *Background*

The study area lies in the region where Durrwood Creek empties into the north-central segment of the Kern River, between latitudes 35°59' N and 36°06' N (Figs. 1 and 2). Bedrock in the region consists of Late Cretaceous intrusive rocks and metamorphic pendant rocks. There are four main intrusive bodies in the study area. In the western half of the study area are the ca. 101 Ma Granodiorite of Brush Creek (Kbc), the ca. 97 Ma Granodiorite of Peppermint Meadow (Kpm), and the ca. 96 Ma Granodiorite of the Needles (Kne) (Fig. 2; Chapter 2). In the eastern half of the study area is the ca. 89 Ma Granite of Castle Rock (Kcr). Between the older granodioritic intrusions and the younger granitic intrusion lies a ~2.5 km wide pendant of metamorphosed Triassic-Jurassic quartz-rich clastic and calcareous continental margin sedimentary rocks (Saleeby and Busby, 1993). They are mapped as units of marble, schist, and quartzite (Mzm, Mzs, and Mzq). Igneous barometry on surrounding intrusive rocks of the study area suggests emplacement at depths of 12–15 km, while the presence of andalusite in metamorphic pendant rocks suggests metamorphic pressures below 13 km depth (Chapter 3).

Ductile fabrics of the PKCF occupy a 2 km wide zone between the Kcr to the east and the pendant rocks, and ductile fabrics of the shear zone are pervasive through the western margin of the Kcr and through much of the pendant (Fig. 3). Small-scale ductile shears are also present, to limited extent, in the eastern margins of the Kne, Kpm, and Kbc to the west. Thus, PKCF fabrics are pervasive in a 2 km wide zone and broadly distributed over a 5 km wide zone in the Durrwood Creek region. The timing of deformation along the PKCF is fairly well constrained to 95-80 Ma, based on zircon U/Pb ages and structural relations of plutons and dikes in the main deformation zone (Busby-Spera and Saleeby, 1990; Chapters 2 and 3). Overprinting the ductile fabrics of the PKCF is the brittle Kern Canyon fault (KCF). Cataclastic rocks of the KCF occupy a narrow zone (cm scale) along the axis of the PKCF (Figs. 1 and 2). The KCF is a latest Cretaceous-Quaternary structure; its movement history is discussed in depth in Chapter 6.

### *Intrusive Rocks*

Plutons in the southern Sierra Nevada have been grouped into five intrusive suites by Saleeby et al. (in press; see Chapter 3 for locations). West of the PKCF in the western half of the study area, the ca. 96-100 Ma Needles intrusive suite comprises the Kbc, Kpm, and Kne. These igneous rocks are predominantly granodioritic in composition and lie primarily to the west of the PKCF (Fig. 2, see Fig. 3 for sample locations). Needles suite intrusive rocks lack overprint from the PKCF for the most part, preserving fairly pristine igneous fabrics. The presence of myrmekitic intergrowths suggest quartz and feldspar interacted at temperatures of  $\sim 600^{\circ}$  C (Fig. 4a; Passchier and Trouw, 2005). A granitic zone in the Kne lies between the pendant in the study area and the KCF. Rocks in

this zone record relatively low-magnitude ductile deformation along the western margin of the PKCF by the kinking of feldspar and patchy extinction in quartz grains (Fig. 4b).

Igneous rocks east of the PKCF are younger and more felsic in composition. The ca. 89 Ma Kcr is a member of the ca. 95–84 Ma Intrusive suite of the Domelands, the most extensive plutonic suite of the southern SNB. The Kcr is distinguished by the presence of pink megacrystic K-feldspar. In contrast to mildly- to non-deformed plutons of the Needles intrusive suite, granitic plutons of the Domelands intrusive suite are pervasively foliated along their western margins. This zone of pervasive foliation in igneous rocks constitutes the eastern margin of the PKCF, and kinematic indicators in this area consistently indicate dextral shear. Fabrics of this zone are described in detail below (see **Structural elements**).

### *Pendant Rocks*

Country rocks of the southern SNB consist of early Mesozoic continental margin sediments that have been severely deformed and metamorphosed. Within the principal damage zone of the PKCF, these rocks have been severely disrupted. Despite this, sedimentary protoliths and primary structures have been recognized and interpreted in domains of low deformation and metamorphic recrystallization (Saleeby et al., 1978). The name Kings sequence was first applied by Bateman and Clark (1974) to Upper Triassic to Lower Jurassic quartzites, carbonates, and locally interstratified metavolcanic rocks between the Dinkey Creek and Mineral King pendants (Fig. 1, ~37° N to ~36° 15' N). Similarities in protolith assemblages of pendants throughout the southern SNB, as well as age correlations of local marine fossils, are strong enough that the Kings sequence

was expanded to include pendants through the southern end of the range (Saleeby et al., 1978). The genetic relation between lithologic units of the Kings sequence is supported by gradational contacts between units and the presence of sedimentary clasts from one unit in an adjacent unit. Pendant rocks along the PKCF are most pertinent to this chapter, and therefore their protoliths constitute the main focus here. The Durrwood Creek study area contains an important segment of the Kern Canyon pendant.

The pendants along the PKCF are, from north to south, the Kern Canyon pendant, the Isabella pendants, and the Tehachapi pendants (Fig. 1). In their present states, these pendants are comprised mainly of interlayered quartzite, phyllite, and schist. Quartzite beds, clasts, and lenses commonly up to 3 m and locally up to 10 m in thickness lie within schist made of quartz + biotite +/- muscovite +/- andalusite +/- hornblende (Fig. 5). The Kern Canyon, Isabella, and Tehachapi pendants also contain layers of calcsilicate rocks (Fig. 6a), local lenses of diamictite as protolith remnants (Fig. 6b), and lenses of marble that stretch over distances of up to 5 km. Local cross-bedding and graded bedding is preserved in the Kern Canyon pendant, as is a quartzite pebble conglomerate (Fig. 7a). The Isabella pendants also contain quartzite pebble conglomerates in several locations, as well as local silicic and metavolcanic rocks (the Erskine Canyon sequence of Chapter 2), and an ~1 km wide zone of amphibolite. After Saleeby et al. (1978), the following protoliths are recognized for the Kern Canyon pendant: thick- to thin-bedded quartzose to subarkosic sandstone with shale and tuff interbeds; thick-bedded limestone; mudstone with tuff, sandstone and limestone interbeds; and basaltic lavas, hyaloclastites and hypabyssals with marl interbeds.

The age of deposition of the Kings sequence is constrained by rare fossils in marbles, calcsilicate rocks, and interbedded epiclastic and volcanoclastic strata of pendants north of the study area. These include Early Jurassic ammonites and Late Triassic bivalves and corals (Saleeby et al., 1978). Late Triassic to Early Jurassic bivalves were found in calcsilicate layers of the Isabella pendant just south of the study area, thereby supporting the regional correlation of Kings sequence rocks along at least an ~150 km long belt of pendants (Saleeby et al., 1978).

Protolith assemblages of pendant rocks in the study area fairly well constrain the environment of deposition of Kings sequence rocks to a shallow to deep marine transition zone. This paleo-environment is discussed in detail in Saleeby et al. (1978), but is briefly summarized here. Relict sedimentary structures that are widespread in studied pendant rocks north of the study area, including graded beds, ripple marks, cross-bedding, rip-up clasts, flame structures, and load casts record a regional-scale depositional environment framework for the Kings sequence. Initial deposition and reworking of flysch was followed by the eastward-increasing appearance of calcareous and epiclastic and volcanoclastic sediments. Shallow-water sands, shales, and carbonates were concentrated east of the flysch sequence, and a shallow-water carbonate reef likely grew along the eastern margin of this sedimentary basin. Thick-bedded quartzites were probably deposited along channels extending from the eastern shallow-water to the western deeper-water facies. In the study area, the regional presence of the same rock types and the local presence of crossbedding and graded bedding in a turbidite sequence of the Kern River pendant (Fig. 7b) support southward extension of the depositional environment described above.

Pendant rocks were pervasively metamorphosed, as described above, by sequential intrusive events at ca. 101, 97, 96, and 89 Ma. They were also variably ductilely deformed and sheared along the PKCF, in the Durrwood Creek study area presumably at the time of intrusion of the Kcr at ca. 89 Ma. The dominant deformation fabric of pendant rocks along the PKCF is that of a protomylonite to mylonite. Kinematic indicators in pendant rocks along the PKCF also consistently indicate dextral shear (Fig. 6b). These fabrics are discussed in detail below (see **Structural elements** and **Strain study**).

#### *The PKCF*

The Proto-Kern Canyon fault, named by Busby-Spera and Saleeby (1990), runs down the middle of the southern SNB and extends north–south for ~130 km, from ~36°10' N to the latitude of the Garlock fault at 35°05' N (Fig. 1). Faulting was localized between the Late Cretaceous igneous plutonic rocks and the Triassic-Jurassic metamorphic pendant rocks described above (Fig. 2). Three phases of evolution took place along this fault system, which together with the later overprinted KCF constitute the Kern Canyon fault system. In the first phase, deformation took place by ductile straining alone, probably at mid-crustal levels, in the 2 km wide zone of the PKSEE. In the second phase, both ductile straining (involving recrystallization) and brittle sliding took place along the fault zone. Finally, brittle sliding took over as the fault was exposed at shallower crustal levels. These three phases are preserved to variable degrees in deformed rocks of the KCF, and suggest a history of deformation during progressive exhumation of the southern SNB.

The earliest stage of deformation along the PKCF involved vertical, east-side-up thrust/reverse displacement that is best preserved in mismatched contours of emplacement depths of plutons in the batholith, and in some rock fabrics of the Durrwood Creek map area and to the south. This early history is discussed in detail in Chapter 3. The second stage of deformation along the PKCF was its main phase of dextral shearing, between ca. 95–80 Ma. This stage is well preserved in macro- and microscopic structures of intrusive igneous and metamorphic pendant rocks of the study area. These structures are described in detail below. Rocks deformed along the PKCF were probably being exhumed as dextral shearing progressed, as is shown by the presence of anastomosing brittle-ductile shears in some rocks (Fig. 8). The third and final stage of deformation along the PKCF in the study area is one of continued dextral shear in the brittle regime, along the KCF. This deformation likely overtook directly the deformation in the ductile regime, as the SNB at this latitude and to the north cooled through 300° C by ca. 80 Ma (Segall et al., 1990; Pachell et al., 2003; Wong, 2005). The KCF is a steeply dipping, narrow ductile–brittle structure that is thought to have had between 6.5 and 13 km of Cretaceous dextral displacement (Moore and du Bray, 1978). The dextral slip history of the KCF is not readily deconvolved from that of the PKCF, but field studies and low-temperature thermochronological data strongly suggest that much of the brittle faulting of the KCF represents superposed late Neogene-Quaternary normal displacements (Nadin and Saleeby, 2001; Chapter 6).

It is clear that structures of the PKCF zone are the product of an extended history of deformation, thus complicating the interpretation and timing of development of the structures developed during the deformation history. In the following section, the

structures and microstructures that characterize the dextral ductile deformation history of the PKCF are described.

### **Structural elements of the PKCF**

#### *General structures*

Orientations of structures within the Durrwood Creek map area are shown on Figure 9, and record 1) vertical ascent of plutons OR early ductile thrusting, 2) dextral north-south oriented strike slip shearing along the PKCF and later KCF, and 3) east-west extension. Foliations in metamorphic pendant and intrusive igneous rocks along the PKCF in the study area strike NNW and generally dip vertically to 65° to both the east and the west (Fig. 9a). These foliations reflect predominantly east-west shortening and north-south as well as vertical stretching during the dextral phase of PKCF activity. Lineation, defined by elongated minerals in the foliation plane, is weakly developed in the pendant rocks. Several small fold axes are also observed throughout the region, generally within the quartzite and marble units. These structures are also oriented north-south, with scattered plunges (Fig. 9b). Steeper plunges of lineation could be early features related to the vertical ascent of plutons in the area, or they could reflect early, west-directed thrusting during the earliest stages of PKCF deformation. Subhorizontal stretching lineations, on the other hand, are related to the dextral shear phase of the PKCF. South of the study area, subhorizontal stretching lineations are common. The small fold axes also represent early vertical deformation followed by subhorizontal, north-south-directed stretching and east-west-directed compression. Finally, structures indicating extension in the area include vertical dikes, joints, cleavage, and small normal

offsets (Fig. 2). These structures are also oriented north-south and dip steeply to vertically east and west (Fig. 9c), suggesting that the extensional features that post-date dextral ductile shearing localized along the pre-existing foliation planes as east–west-directed compression became east-west-directed extension. Indeed, fault scarps along the length of the KCF suggest that normal, west-side-up displacement along this fault took place in Neogene and Quaternary time (Chapter 6). The emphasis in this section is on structural elements that arose during the dominant dextral phase of activity along the PKSEE

### *Kinematic Indicators*

Kinematic indicators are abundant through the Durrwood Creek map area, in both the metamorphic pendant rocks and in the Kcr. These indicators include S-C mylonite fabrics (described below), asymmetric quartz ribbons, deltoid and sigmoid porphyroclasts, and mica “fish” (Fig. 10). These kinematic indicators, which are best preserved in mylonitic foliation, consistently indicate dextral shearing.

### *Mylonites*

The main structure of focus in this chapter is widespread mylonitic foliation, which is distributed through both metamorphic pendant and intrusive igneous rocks along the PKSEE. Mylonites are important because they commonly mark zones of intense non-coaxial (simple shear) deformation. They are best developed in sheared rocks of quartzitic and felsic plutonic compositions, and consist of two foliations that are thought to arise simultaneously (see Berthe et al., 1979). These foliations are a C-surface, or plane

of shearing, commonly defined by aligned, sheared mica grains, and an S-surface, or plane of flattening, commonly defined by the direction of elongation of quartz, feldspar, and micas (Fig. 11).

Mylonites are classified according to the metamorphic grade at which deformation took place, or according to the rock type in which they are developed (see Passchier and Trouw, 2005). In the study area, mylonites are primarily granitic mylonites, quartzite mylonites, calcite mylonites, and phyllite mylonites, or phyllonites. These mylonites developed in greenschist to lower amphibolite metamorphic conditions. The most convincing evidence for this metamorphic grade comes from the presence of andalusite with strong (dextral-sense) preferred orientation in some locations in the metamorphic pendant rocks (Fig. 12). As mentioned earlier, igneous barometric determinations indicate 12–15 km intrusive depths in this region, placing the andalusite-bearing samples at the high-pressure limit of andalusite stability. In the granite mylonites, quartz tends to form elongate ribbons via sub-grain rotation, while feldspar deforms brittlely (Fig. 13a). This type of deformation corresponds to temperatures between 300° C and 400° C (see Passchier and Trouw, 2005), although increased strain rate can reduce the temperature necessary for these deformation mechanisms. One sample of granite mylonite shows feldspar deformed by “bookshelf” fracturing (Fig. 13b), which places the temperature of deformation at ~400° C (Passchier, 1982a; Pryer and Robin, 1996). Shear zone widths on the order of kilometers (as the PKCF is) are considered high-grade shear zones—not in the sense of metamorphic grade, but in extent of mylonitization (Hanmer et al., 1995; Whitmeyer and Simpson, 2003)—but the PKCF in this study area lacks the

ultramylonitic fabrics typical of such high-grade zones. These observations indicate that the PKCF was a medium-grade shear zone in the Durrwood Creek area.

Various elements of mylonitic foliation can be utilized to determine the sense and amount of shear of a shear zone. Firstly, the angle between S- and C-surfaces is a reliable strain indicator. Furthermore, experiments at various conditions have produced strain fabrics via controlled inception of deformation mechanisms. A strain analysis is performed below, comparing experimentally determined deformation mechanisms and conditions to the natural setting of PKCF rocks.

### **Strain and microstructural study**

Studied thin sections from rocks sampled in the Durrwood Creek map area are listed, along with their salient features, in Table 1, and their locations are shown on Figure 3. Samples of quartzite, marble, phyllonite, schist, calcsilicate, diamictite, and mylonitic granite were collected in order to conduct a strain analysis on the different types of deformed rocks. The objective of this study is to examine how strain is distributed through different rock types along the shear zone. In the field, orientations of S- and C-surfaces in mylonites were recorded, where they were measurable, and samples collected were made into thin sections cut perpendicular to and horizontal to foliation.

#### *Shear Strain, Granitic Mylonites*

When C-surfaces begin to form in mylonitic rocks, they are thought to initiate as spaced slip surfaces with the same sense of shear as that of the overall shear zone (Berthé et al., 1979). These surfaces remain aligned parallel to the main shear zone boundary with

progressive deformation. S-surfaces, on the other hand, are initially oriented at  $45^\circ$  to the C-surfaces, and with progressive deformation the angle between these two surfaces decreases into near-parallelism with the shear zone boundary (Ramsay and Graham, 1970; Simpson and Schmid, 1983). The S-surfaces are therefore thought to mark the plane of finite flattening in a shear zone (Ramsay and Graham, 1970).

The changes in orientations of S-surfaces with respect to the orientation of the shear zone boundary, or C-surfaces (Ramsay and Graham, 1970), can be used to analyze shear strain within a shear zone. The difference ( $\theta'$ ) between the strike of the shear zone boundary and strike of the S-surfaces (i.e., the angle between the S- and C-surfaces) within the shear zone are used to determine the shear strain ( $\gamma$ ) within the zone by the following relation:

$$\gamma = 2 / \tan 2\theta' \quad (1)$$

Shear strain was calculated at several points across the PKCF in the granite mylonites, and plotted as a function of distance from the shear zone boundary (Fig. 14). The relationship between  $\theta'$  and  $\gamma$  for measurements in granite mylonites of the Durrwood Creek map area is shown in Figure 14a. The variation of shear strain as a function of distance from the shear zone boundary (taken here as the easternmost map symbol of Fig. 2, where  $\theta' = 45^\circ$ ) is shown in Figure 14b. Up to 1.5 km from the eastern margin of the PKCF, shear strain varies from 0 to 2. Then,  $\sim 1.9$  km from this boundary, the angle between S- and C-surfaces decreases to  $5^\circ$  and shear strain climbs to 11.3. This location, where shear strain is highest, is taken to be the center of the PKCF, which coincides with the contact between the eastern granitic body and the metamorphic pendant rocks. The highest shear strain calculated, when considered over the 15 m.y. span of PKCF activity,

yields a strain rate of  $\sim 10^{-7} \text{ yr}^{-1}$ , which is comparable to that of the modern San Andreas fault (Ward, 1998). However, strain and strain rate probably varied greatly throughout the history of the PKCF. The lack of data between 1.5 and 1.9 km from the shear zone boundary is due to 1) limited access in high-relief, shrub-covered terrain to good outcrops, and 2) difficulty in identifying S- and C-surfaces and measuring their respective attitudes when they are so close to parallel.

#### *Shear Strain, Durrwood Pendant Mylonites*

Metamorphic mylonites in the Durrwood Creek area generally lack the well-developed C-surfaces of the granitic mylonites because they tend to have more a uniform mineral makeup and smaller grains. However, the strain study of Ramsay and Graham (1970) is based on the premise that the variation in  $\theta'$  is simply a variation between the strike of the shear zone boundary and the strike of foliations within the shear zone. Therefore, an estimate is made here of variation in shear strain across the PKCF based on a limited number of foliation orientations with respect to an averaged strike of the PKCF of N 05° E.

The result of the strain analysis that includes foliated pendant rocks is shown in Figure 15. Again, shear strain increases asymptotically with decreasing  $\theta'$  (Fig. 15a). However, in this analysis shear strain is fairly scattered across the PKCF. The angles between shear zone foliations and the shear zone boundary ( $\theta'$ ) vary between 2.9° and 30°, yielding shear strains ( $\gamma$ ) between 1.15 and 19.7 (Figs. 15a and b) reaching a maximum of 19.7 within the pendant rocks 2.3 km west of the eastern boundary of the shear zone. This result is not surprising, as strain is likely to vary not only as a function of

distance, but as a function of the types of rock through which the strain is distributed. It is therefore apparent that within a shear zone that pervades both igneous and metamorphic rocks, strain is heterogeneously distributed with respect to both distance and rock type. It is therefore a worthwhile pursuit to identify strain regimes within the metamorphic pendant rocks of the PKSEE

*Strain Regimes in Metamorphic Pendant Rocks—A Microstructural Study*

The preservation of diagnostic features of deformation regimes along the PKCF may seem fortuitous, but their presence indicates that deformation continued along the shear zone past annealing temperatures. Information on the original grain size of deformed rocks is rarely available. In the Kings sequence rocks along the PKCF in particular, protolith assemblages are well preserved, but are too variable with respect to grain size (i.e., grain sizes in a turbidite sequence can vary from m to  $\mu\text{m}$  scale) to be of much use here. Secondly, deformation mechanisms arising from deviatoric stress and recovery mechanisms resulting from high temperatures are active simultaneously in ductile shear zones. Along the PKCF, preservation of strain features was further obscured by high heat flow from neighboring intruding igneous bodies.

Strain regimes are best studied in quartz aggregates, which will form the core of the strain analysis presented here. But it is useful first to briefly explore strain in other pendant rock types of the shear zone, which include marble, calc-silicate, and pelitic schist. Minimum temperatures for the brittle to ductile transition in mineral deformation are quoted for nominal strain rates of  $10^{-12}$ – $10^{-14}$   $\text{s}^{-1}$ . These minimum temperatures correspond to the limit at which dynamic recrystallization begins. With increasing strain

rate, crystal-plastic deformation temperatures also increase. Given the shear strains calculated above, strain rate along the PKCF at the height of activity would have been  $2 \times 10^{-14} \text{ s}^{-1}$ , but it probably varied significantly throughout the 15 m.y. history of the shear zone.

### *Marble*

Calcite deforms easily, both by mechanical twinning (“even at room temperature,” according to Passchier and Trouw, 2005), and by recrystallization under applied stress. Calcite begins to ductilely deform at temperatures between 200-250° C. The presence of thick ( $>1 \text{ }\mu\text{m}$ ) twin lamellae in all marble samples collected from the Durrwood Creek area indicates calcite deformation occurred in a temperature range of 200°-300° C (Groshong et al., 1984). The progressive stages of calcite deformation that are described by Erskine and Wenk (1998) are recorded in the study area: marble transitions from a coarse-grained ( $>1.5 \text{ mm}$ ), annealed “protolith” (Fig. 16a) to a complexly mechanically twinned and kinked protomylonite (Fig. 16b) to a highly strained, fine-grained ( $25 \text{ }\mu\text{m}$ ) mylonite (Fig. 16c). In pendant rocks along the PKCF, annealed, low- or no-strain textures are found to the west, in proximity to the earlier intrusions. Deformation increases steadily towards the main trace of the PKCF (see Fig. 3 for sample locations).

### *Quartz Aggregates*

Ductility contrasts between minerals results in strain localizing in the weakest mineral phase of a polymineralic rock. In phyllites, mica tends to deform more easily and

to recover (anneal) more quickly than quartz does. In granitic mylonites and in calcsilicates, respectively, feldspar and pyroxene behave brittly at temperatures at which quartz begins to ductilely deform (300° C). An irregular strain pattern through the Kern Canyon pendant therefore arises from contrasting mineral behaviors through heterogeneously distributed rock types. These behaviors are briefly explored below, followed by a more in-depth analysis of strain in quartz-dominant rocks.

### *Phyllite*

In phyllitic rocks, strain is commonly localized in mica, which behaves ductilely above temperatures of 250° C (Stesky et al., 1974), and deforms easily by slip on its planes, kinking, and folding (see Lister and Snoke, 1984). Mica also fractures easily in the brittle regime, and in the study area commonly preserves this phase of deformation more readily than it does the ductile deformation phase. Still, in an environment like that of the PKCF, where heat from surrounding actively intruding plutons probably kept the ambient temperature high, mica regrew with a preferred orientation. This microstructure is a good indication of deformation in a strain field during progressive annealing, and is noted for samples listed in Table 1. A prime example of mica preferred orientation from a phyllonite along the PKCF is shown in Figure 8. This sample can be contrasted with Figure 5a, which shows only a moderate preferred orientation in mica, indicating recovery under lower-strain conditions. The 5a sample is from a location more proximal to the granite–pendant contact than the first sample is, suggesting that high temperatures closer to the heat source persisted as strain lessened, leading to more random alignment of recovering mica in this sample. Perhaps the position of sample D13 (Fig. 5a), in the

strain shadow of a highly deformed marble limb (Fig. 16c), also helped it escape intense deformation.

### *Calcsilicate*

While quartz begins to deform ductilely at 300° C, amphibole and pyroxene behave brittlely through 700° C (see Passchier and Trouw, 2005). This ductility contrast is evident in calcsilicate rocks of the Kern Canyon pendant. In Figure 17a, which is from a local calcsilicate lens in the Kcr (sample D19), quartz is elongate, with irregular boundaries and patchy extinction, while pyroxene has undergone grain size reduction by fracturing. At the northern tip of the pendant, a sample of calcsilicate shows slight elongation of quartz, but indicates an overall low strain field (Fig. 6a). Within the northwestern quadrant of the pendant, both quartz and amphibole lack ductile deformation features (Fig. 17b), although the large amphibole grain in the right-hand side of the field of view of Figure 17b shows evidence for clockwise rotation during brittle fracturing. Based on deformation features in the few samples of calcsilicates from the Durrwood Creek region, it seems that pendant rocks adjacent to the older Kne intrusion were mechanically shielded from high-magnitude strain.

### *Quartzite*

Crystal deformation arising from strain localization in quartz takes place primarily via the mechanisms of bulging recrystallization (BLG), subgrain rotation recrystallization (SGR), and high-temperature grain boundary migration recrystallization (GBM) (Passchier and Trouw, 2005). All of these mechanisms are related in that they reflect the

movement of dislocations through the crystal lattice in an attempt to rid the crystal of internal strain energy. Dislocations glide through the crystal lattice until they reach an obstruction, at which point they can “climb” over that obstruction if temperatures are high enough to localize vacancies near the obstruction. The combination of dislocation glide and climb, dislocation creep, is also often referred to as crystal plastic deformation (see Passchier and Trouw, 2005).

Hirth and Tullis (1992) experimentally identified three regimes of dislocation creep for quartz aggregates, starting from non-deformed quartzite (Fig. 18a). All experiments were conducted under strain rates of  $10^{-6} \text{ s}^{-1}$ . In regime 1, relatively low temperatures ( $700^\circ \text{ C}$ ) yield patchy extinction, inhomogeneously flattened grains, and grain boundary recrystallization (Fig. 18b). At the higher temperatures ( $800^\circ \text{ C}$ ) of regime 2, microstructures are characterized by homogeneously flattened quartz grains with sweeping extinction, and optically visible subgrains (Fig. 18c). At still higher temperatures ( $900^\circ \text{ C}$ ) of regime 3, recrystallization via grain boundary migration is rapid, resulting in relatively large, strain free polygonal grains that may exhibit a shape preferred orientation (Fig. 18d).

Starting in the northwesternmost tip of the field area and proceeding south and east, quartzites in the Durrwood Creek area pendant display microstructures that range from non-deformed through regime 2 of Hirth and Tullis (1992). Sample D31 at the northernmost tip of the pendant is virtually strain-free, or completely recovered via annealing (Fig. 19a). Quartz grains are polygonal, with patchy undulatory extinction. Biotite grains are also non-deformed and scattered with no preferred orientation through the thin section. In contrast, quartz grains in sample D30 (Fig. 19b), which is adjacent to

D31, show heterogeneous flattening and patchy extinction, placing it in regime 1. The contrasting microstructures between proximal samples may be due to the overall smaller grain size in sample D30, or the location of sample D30 within a wider zone of the pendant. Sample D31 also has a large feldspar component, perhaps fortifying the sample as a whole. These two samples are firmly sandwiched within the 96 Ma Kne, which likely acted as a buffer to PKCF strain that took place from 95–80 Ma.

In the thickest width of the Durrwood section of the Kern Canyon pendant, near latitude 36°03' N and just north of the contact between Kpm and Kne (Fig. 2), quartz grains from nearly pure quartzites show little to no deformed microstructures (Fig. 20). Starting on the western side of the pendant, with sample D33, quartz grains are angular, vary in size from 10  $\mu\text{m}$  to 2 mm, and show little to no undulatory extinction. Biotite grains also show no preferred orientation. Just eastward of this location, quartz grains in sample D32 begin to show some patchy undulatory extinction, but they retain their original angular shapes and biotite again shows no preferred orientation in this sample. Proceeding eastward, sample D35 begins to show some signs of strain (Fig. 20) – quartz grain boundaries are serrate, indicating BLG mechanisms of incipient regime 1 microstructures. Micas in this sample are very fine grained and, rather than growing randomly through all parts of the rock, are confined between quartz grains. Samples D36, D37, and D38 all show the same features as D35 (Fig. 20), placing quartzites from this region of the pendant, no matter their distance from the PKCF axis, no higher than regime 1. As with samples from the northernmost tip of the pendant described above, this is likely due to the shielding effect of the surrounding 96 Ma intrusive body.

Microstructures indicate a much higher-grade strain environment (as defined earlier) in the southern half of the pendant, where metamorphic rocks were pinned between earlier intrusive bodies and the younger (89 Ma) Kcr. The proximity to a high heat source during deformation drove quartz into deformation regime 2 (Fig. 21), and indeed all of the quartzites within the southern half of the pendant lie within regimes 1 or 2. Along the southwest margin of the pendant, quartz is heterogeneously flattened and shows patchy undulatory extinction and preferred orientation (Samples D42 and D41, Fig. 21 a). Sample D40 is much finer-grained and mica-rich, and shows homogeneously flattened grains and a strong preferred orientation of both mica and quartz. The most extremely strained quartzite from pendant rocks of the field area is sample D39, which is ~10 m from the contact with Kne (Fig. 3). Quartz grains in this sample show sweeping undulatory extinction, and they are homogeneously flattened (Fig. 21b), indicating regime 2 of Hirth and Tullis (1992).

In order for pendant rocks along the PKCF to enter regime 3 of Hirth and Tullis (1992), temperatures above 900° C would have needed to be reached during deformation along the PKSEE. Temperatures of deformation in the study area must have been below 700° C, as no partial melting is observed. Deformation fabrics of regime 3 would therefore require much lower strain rates than the  $10^{-6} \text{ s}^{-1}$  applied during the Hirth and Tullis (1992) experiments. While strain features are present throughout pendant rocks along the PKCF, they are most evident in regions where temperature was high enough for dislocation creep to begin, but not high enough for it to continue through full recovery and annealing. Quartz microstructural studies in the Durrwood Creek area suggest that

high temperatures near the edge of the 89 Ma intrusive body played a significant role in preservation of deformation features in metamorphic pendant rocks.

The strain studies described at the beginning of this section can be further utilized in an analysis of displacement across the ductile shear zone.

### **Offset along the PKCF**

Some attempts have been made to calculate displacement in shear zones by measuring the changes in orientations of tectonic foliation, or S-surfaces, with respect to the orientation of the shear zone boundary, or C-surfaces (Ramsay and Graham, 1970). Shear strain was determined at several points across a shear zone and plotted as a function of distance from the shear zone boundary. The integral that represents the area under the shear strain-distance curve is used to compute the total displacement ( $s$ ) by the formula:

$$s = \int \gamma dx \quad (2)$$

This method was used to determine displacements along the PKCF on the mesoscopic mapping scale. Figure 22 shows shear strain–displacement curves determined from 1) foliations in igneous mylonites across the eastern 2 km of the PKCF (Fig. 22a), and 2) foliations through both the igneous mylonites and the metamorphic pendant rocks (Fig. 22b). In both estimates, the eastern margin of the PKCF was considered to be the eastern extent of pervasive mylonitization, or where the angle between S- and C-surfaces is at its maximum of  $45^\circ$ , ~2 km east of the contact between the metamorphic pendant rocks and the Kcr (Fig. 2). In the second estimate, lack of a C-surface in the metamorphic

rocks required picking an average orientation of the shear zone, which was taken to be N 05° E, but this, as above, is problematic.

Integrating the area of the curve fitted with a simple trigonometric function in Figure 22a yields a total maximum displacement of 4.2 km for the PKCF in granite mylonites of the Durrwood Creek region. A curve was also fitted, albeit speculatively, for the shear strain versus distance study shown in Figure 15b, which includes shear strains estimated for metamorphic pendant rocks. The integral of this curve yields a total PKCF displacement of 5.2 km (Fig. 22b).

In the study of S-C angle variations in granite mylonites of the PKCF, data are smoothly distributed but form only half of the pattern expected for a shear zone. This is because the other (western) boundary of the shear zone resides in the metamorphic pendant rocks. Therefore, an estimate of displacement exclusively for granite mylonites was made by mirroring the curve where data were lacking. This extrapolated curve therefore yields an estimated offset for a shear zone that resides exclusively in granite mylonites, which is not the case. Therefore, although the curve is better fit for the half-shear zone shown in Figure 22a, the greater displacement estimate calculated for the shear zone in both granite mylonites and metamorphic pendant rocks is the more reasonable one.

It is evident in Figure 22b that the curve-fitted data for both granite mylonites and metamorphic pendant rocks are scattered. There are several possible reasons for this. Firstly, the method described above was applied by Ramsay and Graham (1970) at thin section and outcrop scales, and in this study it was applied to a 2.5 km wide zone. Secondly, the PKCF is a zone of heterogeneously distributed shear, as the strain study

may suggest. Although the heterogeneous nature of shear zones is taken into account by the Ramsay and Graham (1970) method, on thin section to outcrop scales this heterogeneity refers to a zone in which foliation angles with respect to the shear zone boundary increase continuously toward the center of the shear zone, and decrease continuously toward its outer edge. In other words,  $\theta'$  decreases from some angle at one boundary of the shear zone to zero toward the center of the shear zone, and then increases toward the other boundary of the shear zone. In the overall PKCF zone, shear strain is most accurately described as distributed across a wide zone within which several smaller-scale, higher-strain zones reside. The PKCF likely widened to a broad zone with progressive deformation along relatively narrow zones of ductile deformation. Strain is also distributed in small-scale domains outside of the main PKCF zone, and as such, the true shear zone boundary is difficult to pinpoint. An estimate of its edge for use in the above equation was based on diminished pervasive shear. The domainal shears outside of the main PKCF zone may contribute somewhat to total displacement: Along hundreds to thousands of these small domainal shears, several meters of displacement may accrue.

It is useful to compare the displacement calculated from the curves in Figure 22 to other displacements estimated for shear zones of a similar scale. Mitra (1979) used the method described above, as well as the measurement of principal strain directions from thin sections of stretched mineral grains, to derive a relationship between the width of deformation zones ( $w$ ) and the displacements on them:

$$s = 2w^{1.05} \quad (3)$$

For the PKCF width of 2.5 km, this relationship yields a total displacement of 5.23 km, which is in agreement with the estimate derived from the study including foliations from

both metamorphic pendant rocks and granite mylonites. Therefore, displacement along the PKCF in the Durrwood Creek region is estimated at 5.2 km.

### **Discussion and Conclusions**

The igneous and metamorphic rocks along the PKCF record the history of broadly and heterogeneously distributed strain. The structures and microstructures that document these variations are the product of an extended deformation history that may have originated with vertical, east-side-up reverse or thrust motion (Chapter 3). This earliest phase of the PKCF could be recorded in the steeply plunging lineations of pendant rocks in the northern reaches of the shear zone. In this region, the main, dextral strike-slip phase of PKCF activity left the dominant signature in small folds and other kinematic indicators. Dextral ductile shearing along the PKCF was pinned between the western margin of the 89 Ma Granite of Castle Rock and Mesozoic Kings sequence metamorphic pendant rocks (Fig. 2). This deformation took place at depths of ~12 km, in greenschist to lower amphibolite facies, as indicated by metamorphic index minerals and deformation behavior of key minerals such as quartz and feldspar.

The temperatures under which deformation occurred and was preserved are more difficult to pinpoint. Ductile behavior in quartz and brittle behavior in feldspar at normal strain rates of  $10^{-12}$ – $10^{-14}$  s<sup>-1</sup>, which are similar to the strain rates calculated for the PKCF, place temperature of deformation at ~400° C (see Passchier and Trouw, 2005) in granitic mylonites of the eastern edge of the PKCF. The absence of granulite facies metamorphism in the study area restricts deformation temperatures to below 700° C, but comparison of thin section samples of deformed quartzite from the Durrwood Creek map area with

experiments that define quartz creep regimes (Hirth and Tullis, 1992) suggests that temperatures during deformation could have reached as high as 600° C in metamorphic pendant rocks in contact with the 89 Ma Granite of Castle Rock. However, the Hirth and Tullis (1992) experiments were performed at strain rates of  $10^{-6} \text{ s}^{-1}$ , far higher than strain rates calculated for the PKCF. At lower strain rates, lower temperatures can result in the same deformation features as formed under high strain rates and high temperatures.

The interplay of temperature and strain rate complicates the analysis of strain-related microstructures in fossil ductile shear zones. Nonetheless, a study of relative strain through the width of a shear zone can shed light on how deformation is localized and distributed through different rock types. This study was undertaken for rocks of the Kern Canyon pendant in the Durrwood Creek area both as a function of rock type and as a function of proximity to the heat source during PKCF dextral ductile shearing. With few exceptions, all pendant rock types show the same relationship of higher-strain fabrics closer to the contact of the pendant with the 89 Ma intrusive body.

Calcite from marble within the portion of the pendant surrounded by the 96 Ma Granodiorite of the Needles and marble in proximity to the 97 Ma Granodiorite of Peppermint Meadow (Fig. 1a) forms coarse, interlocking crystals (Fig. 16a). The only evident deformation microstructure in these marbles is twin lamellae, which form even at low temperatures (200° C) and under low stress. With increasing proximity to the main trace of the PKCF, microstructures in marble show increasing evidence of strain. Halfway between the 101 Ma Granodiorite of Brush Creek and the PKCF, calcite is complexly twinned and kinked, forming a marble protomylonite (Fig. 16b). Marbles

closest to the boundary with the 89 Ma Granite of Castle Rock suffered the most damage from the PKCF, becoming marble mylonite (Fig. 16c).

Marble shows the clearest relationship between strain and proximity to the main trace of the PKCF because this rock type deforms easily. The other pendant rocks consist of quartz aggregates, including phyllites, calcsilicates, and quartzite. As with the marble samples from the map area, phyllites and calcsilicates are variably strained in relation to their distances from the contact with the Kcr. However, the stronger components and weaker components of these rocks, respectively, cause partitioning of strain into the weakest minerals. In the northernmost tip of the pendant, quartz in calcsilicate rock is deformed ductilely while pyroxene is deformed brittlely (Figs. 6a and 17). One sample from a calcsilicate lens within the Kcr shows ductile deformation of quartz and brittle deformation in pyroxene, while a sample from the northwestern segment of the pendant is virtually strain-free. The same relation is seen in the phyllites: Concentration of deformation in weaker biotite is evident in the strong preferred orientation of this mineral (Fig. 8). However, phyllites sampled near the contact with Kcr show little preferred orientation of biotite (Fig. 5a), suggesting that recrystallization in these minerals at  $\sim 200^{\circ}$  C possibly post-dated high strain along the PKCF. It would be worthwhile to try to date some of the micas from these samples.

Nearly pure quartzite from pendant rocks along the PKCF provided the opportunity to classify deformation in to the dislocation creep regimes outlined by Hirth and Tullis (1992). These samples clearly demonstrate the temperature dependence of deformation. Within the northern segment of the pendant, where pendant rocks are sandwiched within the 96 Ma Granodiorite of the Needles, quartz is virtually strain-free.

Approaching the eastern side of the pendant and the PKCF, quartz enters strain regime 1. In the southern half of the pendant, where pendant rocks were pinned between the actively deforming 89 Ma Granite of Castle Rock to the east and the solidified 101–97 Ma granodiorite bodies to the west, deformation microstructures show increasingly higher grades to the east (Figs. 19 and 20), reaching regime 2 right at the contact with the Kcr (Fig. 21b).

By combining strain studies with timing of offset previously established for activity along the PKCF (Busby-Spera and Saleeby, 1990; Chapters 2 and 3), it is possible to estimate a strain rate for the PKCF of  $\sim 10^{-7}$  yr<sup>-1</sup>, which is similar to the strain rate along the modern San Andreas fault (Ward, 1998). Although the strain rate calculated for the PKCF agrees with those determined for modern analogues of strike-slip faults, strain likely varied not only with time but also within the different rock types along the PKCF, as shown in the microstructural study and as summarized above.

Strain across the foliated rocks of the PKCF was also used to estimate offset along the zone. A study of the varying angles between S- and C-surfaces within the granite mylonite as a function of distance from the eastern shear zone boundary yields  $\sim 4$  km of offset. An analysis of foliation angles (S-surfaces) through both granite mylonites and deformed metamorphic pendant rocks yields a displacement of 5.2 km. This result is in good agreement with studies showing variation in displacement as a function of the width of a shear zone (Mitra, 1979).

By combining the strain and microstructural studies, a preliminary model of initiation and development can be built for the PKCF. Igneous intrusions at ca. 101, 97, and 96 Ma partly surrounded and metamorphosed Mesozoic Kings sequence quartz-rich

shallow-to-deep marine sediments. This environment cooled over the following 7 m.y., after which the Granite of Castle Rock intruded to the east of the pendant at 89 Ma. The overall strain regime of the SNB at this time was transpressive, and this led to the development of several early thrusts followed by later strike-slip ductile fault zones through the batholith (Chapter 3). In the Durrwood Creek map area, deformation localized along the contact between the metamorphic pendant rocks and the 89 Ma intrusive. Rocks along this contact are pervasively sheared. In the Kcr, mylonitic fabric dies out progressively eastward over 2 km. Deformation features pervade the pendant rocks in the southern half of the field area. The northern half of the pendant escaped pervasive ductile deformation because it was buffered by the surrounding, older Granodiorite of the Needles. A scenario can be erected in which ductile deformation began along several weak, narrow zones both within the pendant (along the marble, for instance) and at the contact between the pendant to the west and Kcr to the east. As deformation progressed, these zones widened through the pendant in its southern half and in the western edge of the Kcr. Ultimately, as temperatures and strain rates in this region fell, deformation related to PKCF activity broadened to a 2-3 km wide zone that included the 1 km width of the southern half of the pendant, and 2 km of the western edge of the Kcr. As this part of the batholith was exhumed and cooled below 300° C, by ca. 80 Ma, dextral slip continued along the brittle KCF. Thus, the KCF system documents the evolution of a midcrustal shear zone from a weak, probably narrow, zone to a kilometer-scale region of broadly distributed shear, and finally to a thin zone of brittle deformation over the span of 20 m.y.

## References

- Bateman, P. C., and Clark, L. D., 1974, Stratigraphic and structural setting of the Sierra Nevada batholith: *Pac. Geol.*, v. 8, p. 78-89.
- Berthe, D., Choukroune, P., and Jegouzo, P., 1979, Orthogneiss, mylonite, and non-coaxial deformation of granites: the example of the south Armorican shear zone: *Jour. of Struct. Geo.*, v. 1, p. 31-42.
- Busby-Spera, C. J., and Saleeby, J. B., 1990, Intra-arc strike-slip fault exposed at batholithic levels in the southern Sierra Nevada, California: *Geology*, v. 18, n. 3, p. 255-259.
- Engebretson, D. C., Cox, A., and Gordon, R.G., 1985, Relative motions between oceanic and continental plates in the Pacific Basin: *Geol. Soc. of Amer. Spec. Pap.*, v. 206, 59 pp.
- Erskine, B. G., and Wenk, H.-R., 1998, Preferred orientation and microstructure of mylonitic carbonate rocks, in Snoke, A. W., Tullis, J., and Todd, V. R., eds., Fault-Related Rocks: Princeton University Press, p. 378-379.
- Greene, D. C., and Schweickert, R. A., 1995, The Gem Lake shear zone: Cretaceous dextral transpression in the northern Ritter Range pendant, eastern Sierra Nevada, California: *Tectonics*, v. 14, n. 4, p. 945-961.
- Groshong, Jr R. H., Teufel, L.W., and Gasteiger, C., 1984, Precision and accuracy of the calcite strain-guage technique: *Geol. Soc. of Amer. Bull.*, v. 95, p. 357-363.
- Hanmer, S., Williams, M., and Kopf, C., 1995, Modest movements, spectacular fabrics in an intracontinental deep-crustal strike-slip fault: Striding-Athabasca mylonite zone, NW Canadian Shield: *Jour. of Struct. Geo.*, v. 17, n. 4, p. 493-507.
- Hirth, G., and Tullis, J., 1992, Dislocation creep regimes in quartz aggregates: *Jour. of Struct. Geo.*, v. 14, p. 145-160.
- Lister, G. S., and Snoke, A. W., 1984, S-C mylonites: *Jour. of Struct. Geo.*, v. 6, n. 6, p. 617-638.
- Mitra, G., 1979, Ductile deformation zones in Blue Ridge basement rocks and estimation of

- finite strains: *Geol. Soc. of Amer. Bull.*, v. 90, p. 935-951.
- Moore, J. G., and du Bray, E., 1978, Mapped offset on the right-lateral Kern Canyon fault, southern Sierra Nevada, California: *Geology*, v. 6, n. 4, p. 205-208.
- Nadin, E. S., and Saleeby, J. B., 2001, Relationships between the Kern Canyon Fault (KCF) and the Proto-Kern Canyon Fault (PKCF), Southern Sierra Nevada, CA: *EOS Transactions*, v. 82, n. 47.
- Pachell, M. A., Evans, J. P., and Taylor, W. L., 2003, Kilometer-scale kinking of crystalline rocks in a transpressive convergent setting, central Sierra Nevada, California: *Geol. Soc. of Amer. Bull.*, v. 115, n. 7, p. 817.
- Passchier, C. W., and Trouw, R. A. J., 2005, Microtectonics: Springer Verlag, 366 pp.
- Pryer, L. L., and Robin, P. Y. F., 1996, Differential stress control on the growth and orientation of flame perthite: a paleostress direction indicator: *Jour. of Struct. Geo.*, v. 18, p. 1151-1166.
- Ramsay, J. G., and Graham, R. H., 1970, Strain variation in shear belts: *Can. Jour. of Earth Sci.*, v. 7, p. 786-813.
- Rolandone, F., and Jaupart, C., 2002, The distributions of slip rate and ductile deformation in a strike-slip shear zone: *Geophys. Jour. Inter.*, v. 148, p. 179-192.
- Saleeby, J., Goodin, S., Busby, C., and Sharp, W., 1978, Early Mesozoic paleotectonic-paleogeographic reconstruction of the southern Sierra Nevada region: *AAPG Bull.*, v. 62, n. 11, p. 2361-2362.
- Saleeby, J. B., and Busby-Spera, C. J., 1993, Paleogeographic and tectonic setting of axial and western metamorphic framework rocks of the southern Sierra Nevada, California, *in* Dunne, G., and McDougall, K., eds., Mesozoic Paleogeography of the Western United States-II: *Pacific Section SEPM*, Book 71, p. 197-226.
- Segall, P., McKee, E. H., Martell, S. J., and Turin, B. D., 1990, Late Cretaceous age of fractures

- in the Sierra Nevada Batholith, California: *Geology*, v. 18, n. 12, p. 1248.
- Simpson, C., and Schmid, S. M., 1983, An evaluation of criteria to deduce the sense of movement in sheared rocks: *Geol. Soc. of Amer. Bull.*, v. 94, p. 1281-1288.
- Stesky, R. M., Brace, W. F., Riley, D. K., and Robin, P. Y. F., 1974, Friction in faulted rock at high temperature and pressure: *Tectonophys.*, v. 23, p. 177-203.
- Teyssier, C., Dunlap, W. J., and Karato, S.-I., 1991, Propagation of ductile deformation in a thrust system: Structural and radiometric evidence and tectonic implications, in *Terra Abstracts, Mechanical Instabilities in Rocks and Tectonics*, Montpellier, France, p. p. 39.
- Tikoff, B., and Greene, D., 1997, Stretching lineations in transpressional shear zones: An example from the Sierra Nevada Batholith, California: *Jour. of Struct. Geo.*, v. 19, n. 1, p. 29-39.
- Tikoff, B., and Saint Blanquat, M., 1997, Transpressional shearing and strike-slip partitioning in the Late Cretaceous Sierra Nevada magmatic arc, California: *Tectonics*, v. 16, n. 3, p. 442-459.
- Tobisch, O. T., Saleeby, J. B., Renne, P. R., McNulty, B., and Tong, W. X., 1995, Variations in Deformation Fields During Development of a Large- Volume Magmatic Arc, Central Sierra-Nevada, California: *Geol. Soc. of Amer. Bull.*, v. 107, n. 2, p. 148-166.
- Ward, S. N., 1998, On the consistency of earthquake moment rates, geological fault data, and space geodetic strain: the United States: *Geophys. Jour. Int.*, v. 134, p. 172-186.
- Whitmeyer, S. J., and Simpson, C., 2003, High strain-rate deformation fabrics characterize a kilometers-thick Paleozoic fault zone in the eastern Sierras Pampeanas, central Argentina: *Jour. of Struct. Geo.*, v. 25, p. 909-922.
- Wong, M. S., 2005, Structural evolution of mid-crustal shear zones: Integrated field and thermochronologic studies of the Sierra Mazatán metamorphic core complex, Sonora, Mexico and the Proto-Kern Canyon dextral shear zone, southern Sierra Nevada, California: *PhD Thesis*, University of California, Santa Barbara, 175 pp.

## Figure Captions

1. Location map of the southern Sierra Nevada batholith, showing plutonic igneous rocks and their interstitial metamorphic pendant rocks. Local and regional faults are shown as well.
2. Geologic map of the Durrwood Creek map area.
3. Sample location map for samples discussed throughout text. Refer to Figure 2 for map details.
4. Granodiorite, showing strain-free texture of sample D1 and mildly deformed texture of sample D3. a) Sample D1 shows myrmekitic intergrowth (M) of feldspar and quartz, indicative of  $T \sim 600^\circ \text{C}$ . b) Kinked feldspar (F) and patchy extinction in quartz (Q) indicates low strain in sample D3.
5. Schists of the Kern Canyon pendant. a) Biotite (B) + quartz (Q) from sample D13. b) andalusite (A), rimmed by fine-grained muscovite from sample D17. See Figure 3 for sample locations.
6. a) Local calcsilicate, with pyroxene (P) and quartz (Q); sample D18, and b) Local diamictite, with larger quartzite clast in finer-grained matrix of quartz and mica (M); sample D10. Arrows indicate dextral sense of shear in quartz clast, as does preferred orientation of quartz grains in the clast, indicated by the black line.
7. Relatively nonmetamorphosed Kings sequence protoliths. a) Quartz pebble conglomerate. b) Turbidite sequence, showing fining of sediment size from bottom right to upper left of photo.

8. Anastomosing brittle-ductile shears of sample D11. Ductile shearing is defined by aligned micas (M), while through-going cracks form the brittle shears. View is plane polarized light.
9. Lower hemisphere, equal area stereonet projections of fabric elements within the Durrwood Creek area of the Kern Canyon pendant. A) Poles to foliation dip steeply east and west, and strike north-south. B) Plunges of lineations and small fold axes are mostly steep, but some are sub-horizontal. Lineations are light grey circles, small fold axes are black circles. C) Poles to fracture, joints, and small normal faults along the PKCF. Steep east and west dips and north-south strikes indicated reactivation of initial ductile strain fabrics in the brittle regime.
10. Biotite mica (M) “fish” indicating dextral ductile shear in samples a) D4 and b) D6. Arrows indicate sense of shear.
11. S-C granite mylonite. S-planes, or planes of flattening, are defined by elongate feldspar. C-planes, or planes of slip, are defined by aligned mica. The smaller the angle between S- and C-surfaces, the higher the shear strain the mylonite experienced.
12. Andalusite schist, sample D16. The presence of opaque mineral inclusions in andalusite (a) indicates greenschist to lower amphibolite facies metamorphic grade. Some andalusite grains show rotation and growth in a dextral shear regime, as indicated by the arrows.
13. Granite, showing a) ductile flow of quartz (Q) in contrast with brittle deformation of feldspar (F), indicating deformation T of 300°–400° C in sample D5, and b) “bookshelf” microfracturing of feldspar (F), indicating deformation T ~400° C in sample D6.
14. Shear strain study, S-C granite mylonites. a) Shear strain varies as a function of the angle between S- and C-planes. b) Shear strain vs. distance eastward across the granitic mylonites of Kcr.

15. Shear strain study of metamorphic pendant rock foliations across the PKCF. a) Variation of shear strain as a function of the angle between foliation and the shear zone boundary. b) Shear strain vs. distance from west to east across the pendant rocks.
16. Marble samples, showing progressive stages in deformation. All sections are pure calcite, taken in cross-polarized light. a) Annealed fabric with thick twin lamellae indicating deformation T of 200° - 300° C. b) Complex twinning and kinking of calcite grains and grains size reduction in a marble protomylonite. c) High-grade marble mylonite has very small calcite grains with larger, stretched calcite “porphyroclasts” (P).
17. Calcsilicate. a) Fine-grained rock from a lens within the eastern granite, showing ductilely deformed quartz (Q) and brittlely deformed (highly birefringent) pyroxene (Px). b) Amphibole porphyroclast (A) deforms brittlely during clockwise rotation. The continuity of the grain is seen in plane polarized light (top photo), while its broken edges are seen in cross-polarized light (bottom photo). Arrow indicates direction of shear is clockwise, or right lateral. Quartz is not deformed in this sample.
18. Quartz dislocation creep regimes of Hirth and Tullis (1992). a) Non-deformed start sample, showing sharp grain boundaries, no preferred orientation of grains, and no undulatory extinction. b) Regime 1, deformed at 700° C and  $10^{-6} \text{ s}^{-1}$ , shows heterogeneously flattened grains and patchy undulatory extinction. (Horizontal cracks arose during unloading.) c) Regime 2, deformed at 800° C and  $10^{-6} \text{ s}^{-1}$ , shows homogeneously flattened grains with sweeping undulatory extinction. d) In regime 3, deformed at 900° C and  $10^{-6} \text{ s}^{-1}$ , 100% recrystallization has rid the grains of dislocations.
19. Quartzite from the northernmost tip of the pendant. a) Relatively coarse quartz grains (shades of gray) are virtually strain-free, showing only patchy undulatory extinction. Biotite (B) shows no preferred orientation. Sample D31. b) Finer-grained quartz is ductilely deformed in regime 1 of Hirth and Tullis (1992), as seen by heterogeneous flattening and patchy undulatory extinction. Sample D30.

20. Quartzite from the northern half of the pendant. Both samples are composed primarily of quartz. a) Sample D35, from the western side of this section, shows marginal patchy extinction and grain flattening, indicating incipient regime 1 deformation. b) Grain boundaries from sample D38, closer to the main trace of the PKCF, are sharp, indicating no strain. Quartz in this sample also has little to no undulatory extinction.

21. Quartzite from the southern half of the pendant. All samples shown are composed primarily of quartz, and are cut perpendicular to foliation. a) Quartz grains in samples D41 and D42 show heterogeneous flattening and patchy undulatory extinction of regime 1. b) Quartz grains in sample D39, from the easternmost edge of the pendant in this segment, show the heterogeneous flattening and sweeping undulatory extinction of regime 2. This is the highest-grade quartzite mylonite from the pendant in the Durrwood Creek area.

22. Curves fitted to calculations of shear strain (y-axis) as a function of distance (x-axis) across the width of the PKCF. The area under the curve represents total displacement along the shear zone. a) Shear strain measured from angles between S- and C-surfaces of granite mylonites. Displacement = 4.2 km. b) Shear strain calculated from angles between foliation (in both metamorphic pendant rocks and granite mylonite) and an average strike of the PKCF of N05E. Displacement = 5.2 km.

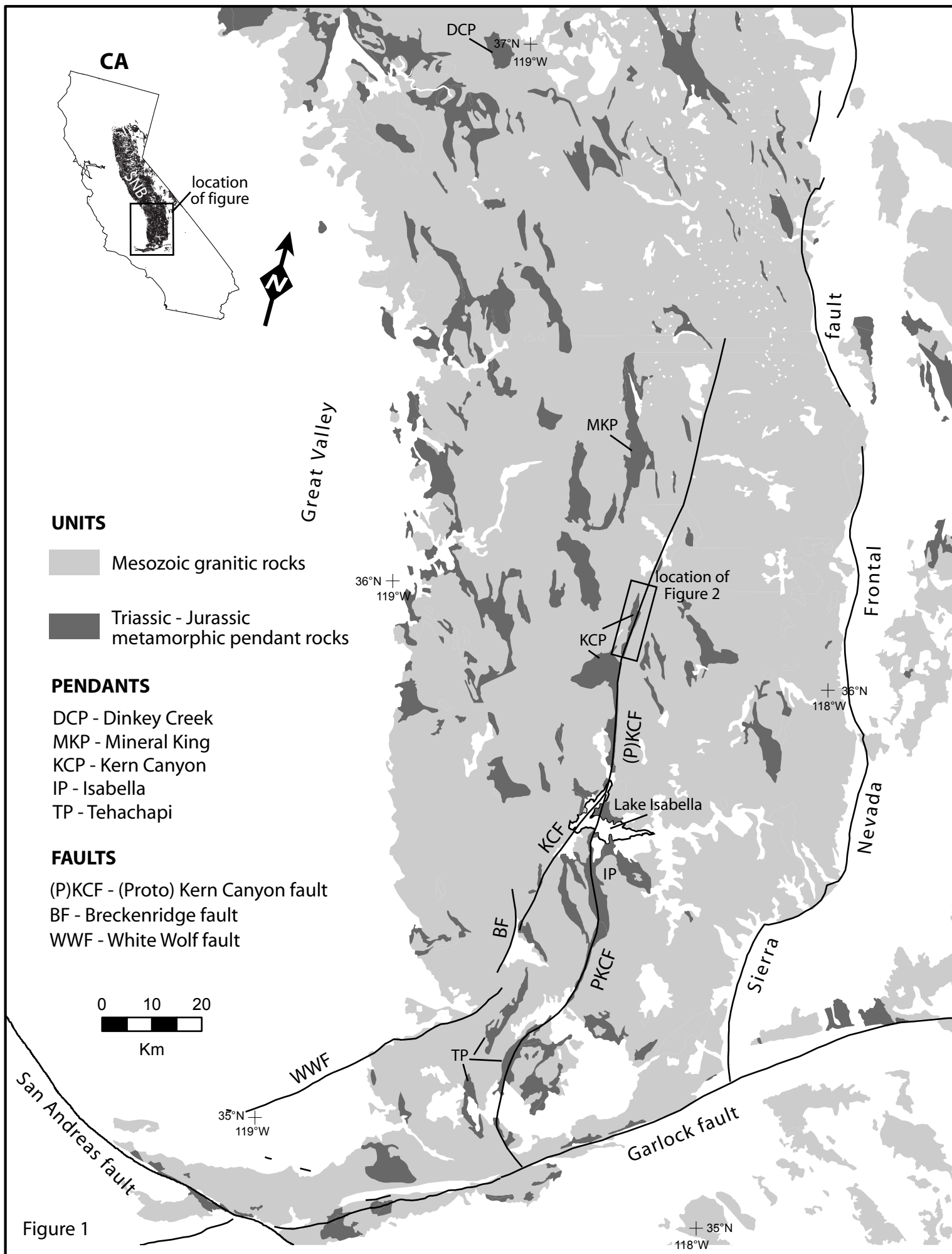


Figure 1

# Detailed Geologic Map of the Durrwood Creek and north Fairview Quadrangles, Kern County, California

by E.S. Nadin

## LEGEND

### Units

#### Tertiary volcanic rocks and alluvium

- Qal Quaternary alluvium and debris flows
- Qr Quaternary rubble of eroded basalt
- Tb Tertiary basalt, ca 3 Ma

#### Cretaceous intrusive rocks

- Kcr Granite of Castle Rock, ca 89 Ma
- Kne Granodiorite of the Needles, ca 96 Ma
- Kpm Granodiorite of Peppermint Meadow, ca 97 Ma
- Kbc Granodiorite of Brush Creek, ca 101 Ma

#### Jurassic - Triassic pendant rocks

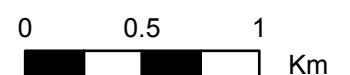
- Mzm Mesozoic marble
- Mzs Mesozoic schist - variably metamorphosed and strained calcsilicate, micaceous quartzite, and phyllite.
- Mzq Mesozoic quartzite - local pure quartzite pods and lenses

### Contacts

- certain
- - - approximate
- - - - - inferred from aerial view
- ..... concealed
- ? - ? - ? - uncertain
- fault, certain
- - - fault, approximate
- ..... fault, concealed
- ~ ~ shear zone overprint (PKCF)

### Symbols

- strike of igneous foliation, dipping and vertical
- strike of metamorphic foliation, dipping and vertical
- strike of mylonitic foliation, dipping and vertical
- trend and plunge of lineation
- trend and plunge of small folds, tight, open, and dextral
- small normal offset
- strike of jointing, dipping and vertical
- strike of cleavage, dipping and vertical
- strike of vertical dike



contour interval 40 feet

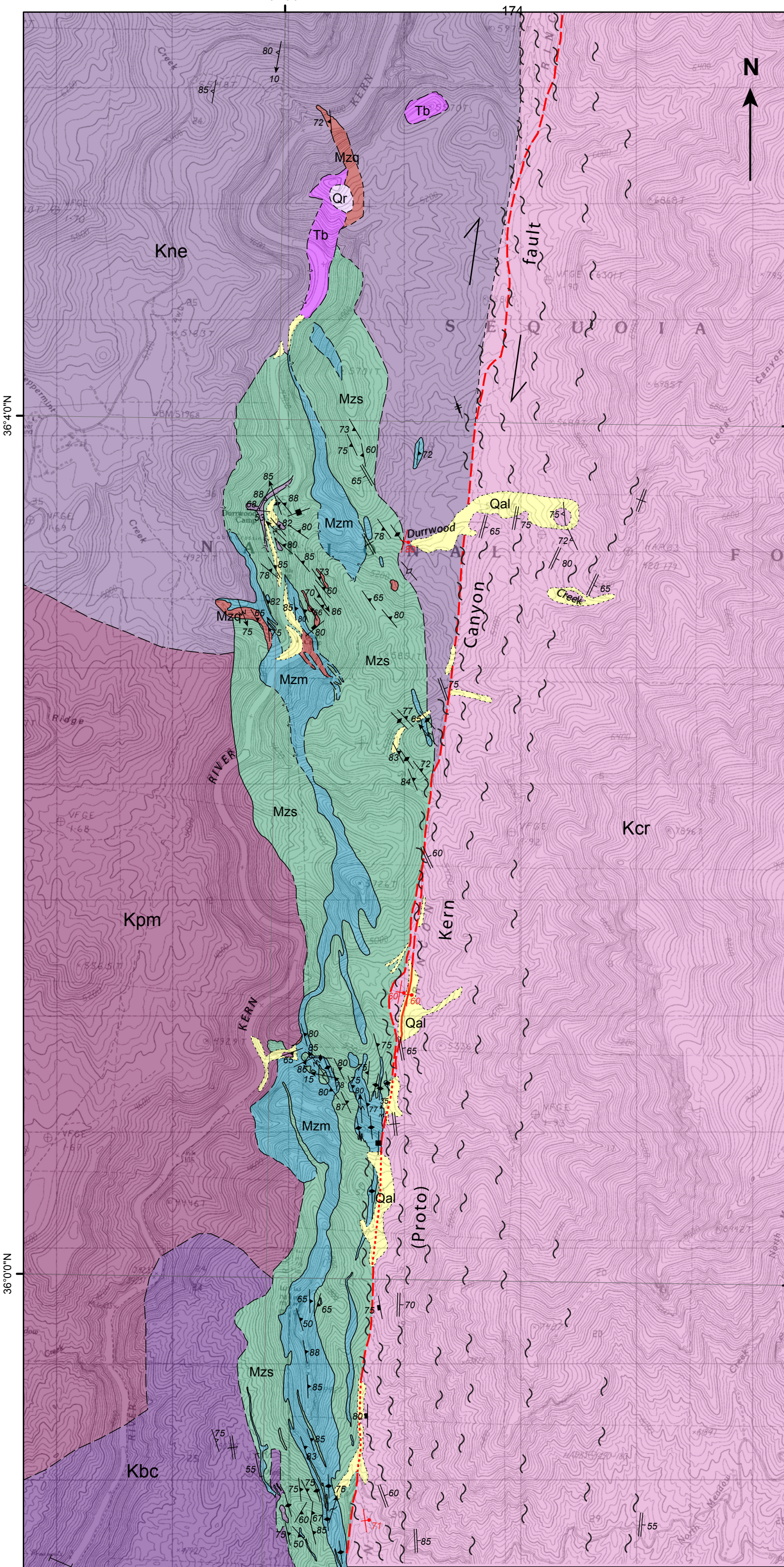


Figure 2

118°28'0"W

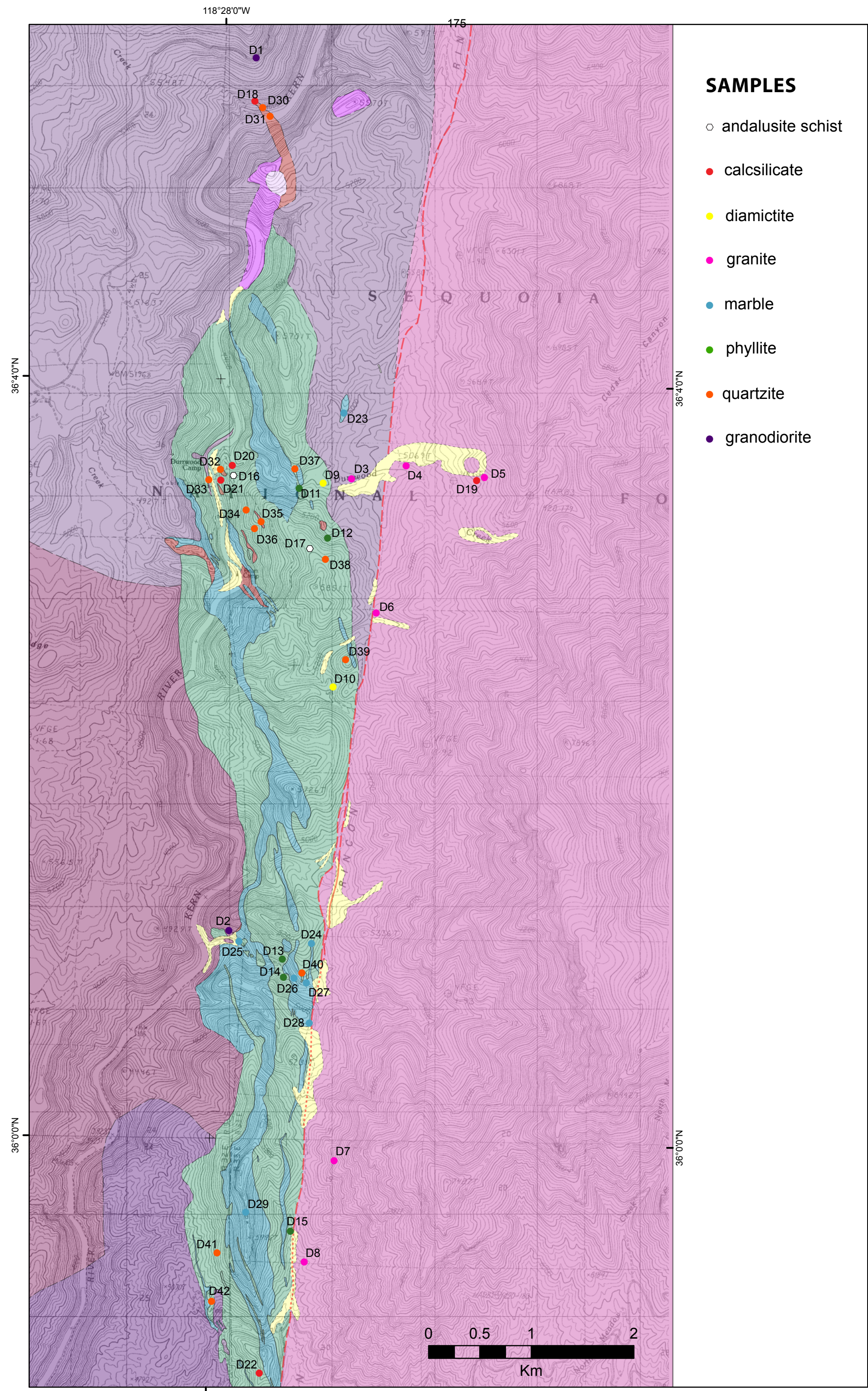


Figure 3

118°28'0"W

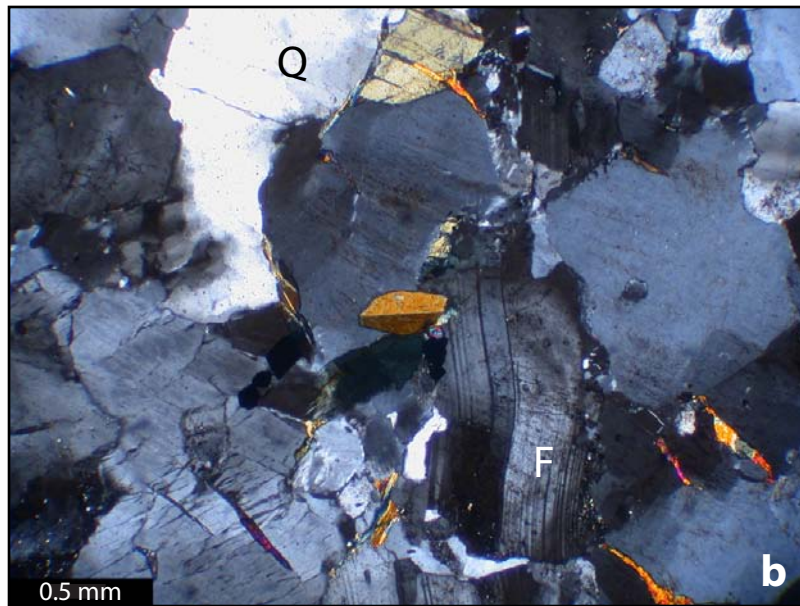
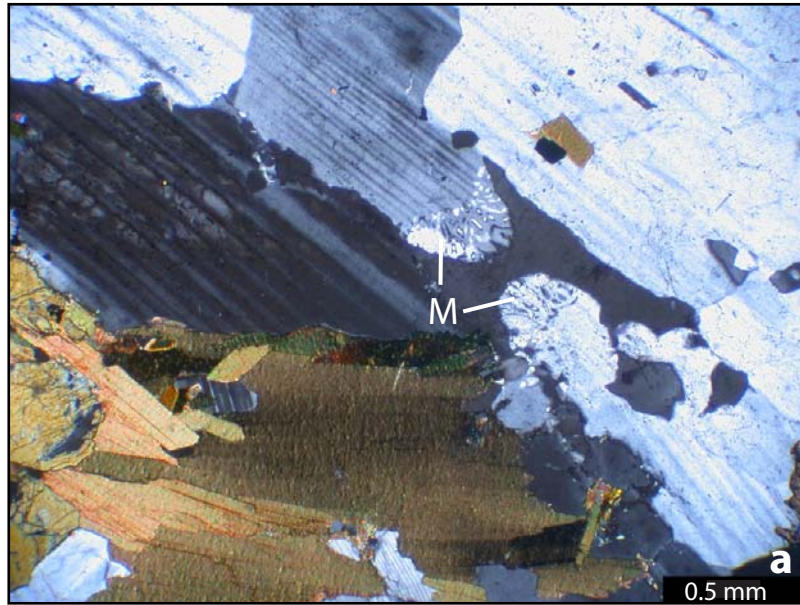


Fig 4. Granodiorite, showing strain-free texture of sample D1 and mildly deformed texture of sample D3. a) Sample D1 shows myrmekitic intergrowth (M) of feldspar and quartz, indicative of  $T \sim 600^\circ \text{C}$ . b) Kinked feldspar (F) and patchy extinction in quartz (Q) indicates low strain in sample D3.

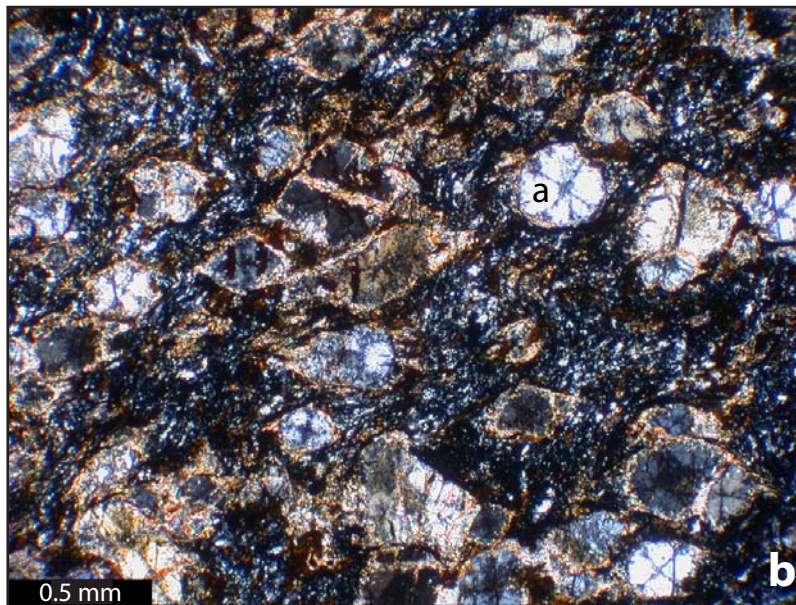
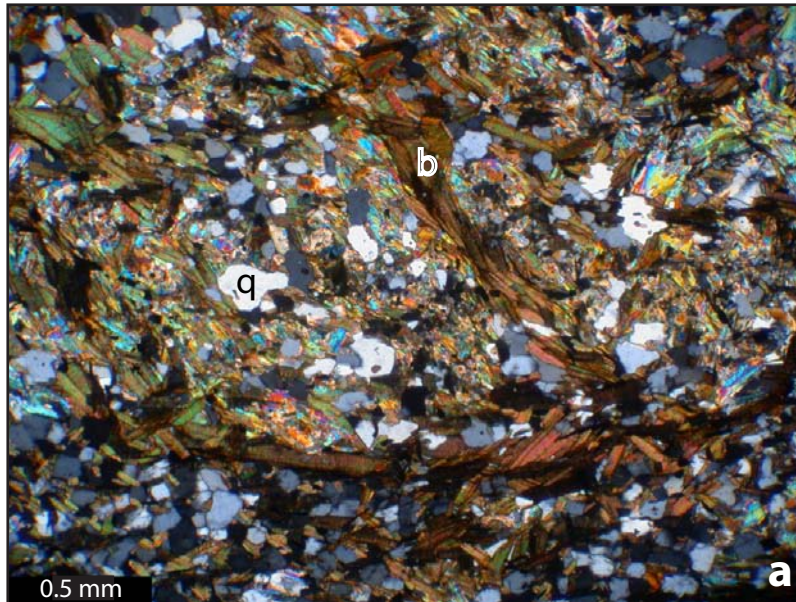


Fig 5. Schists of the Kern Canyon Pendant. a) Biotite (b) + quartz (q) from sample D13. b) andalusite (a), rimmed by fine-grained muscovite from sample D17. See Figure 3 for sample locations.

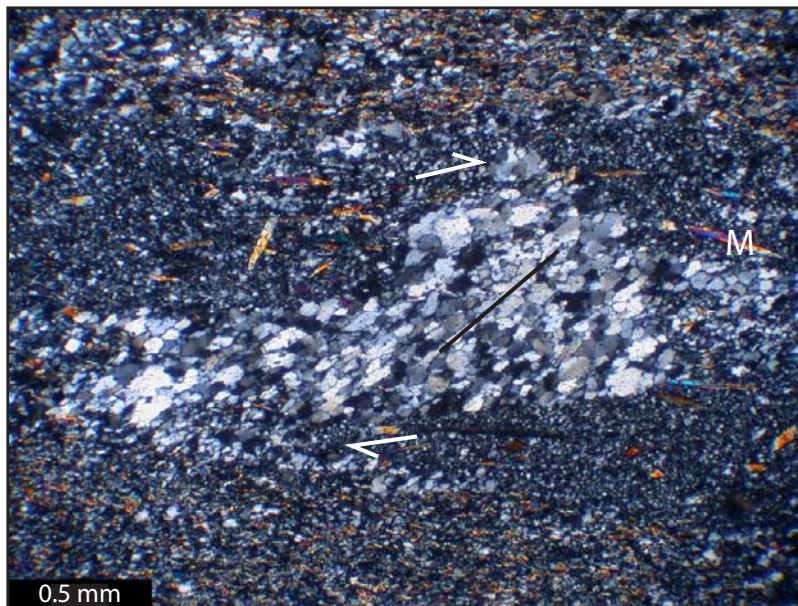
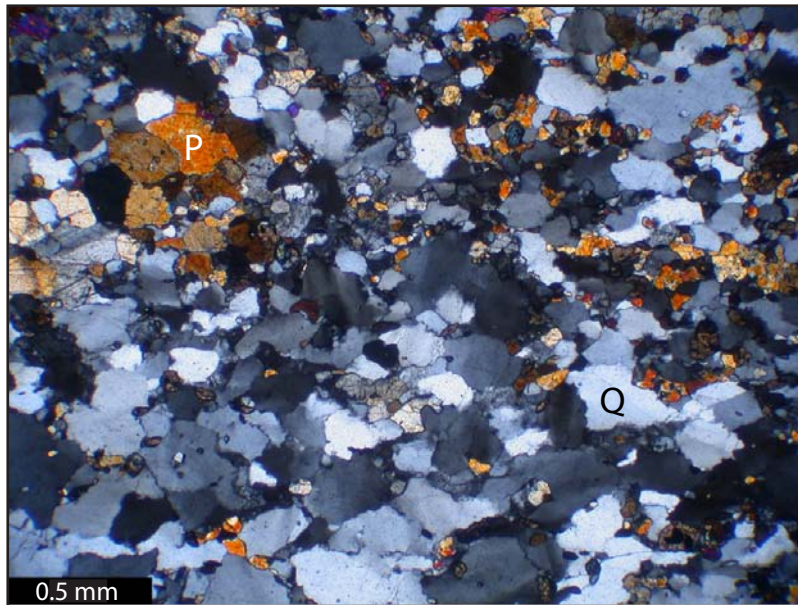


Fig 6. a) Calc-silicate, with pyroxene (P) and quartz (Q); sample D18, and b) Diamictite, with larger quartzite clast in finer-grained matrix of quartz and mica (M); sample D10. Arrows indicate dextral sense of shear in quartz clast, as does preferred orientation of quartz grains in the clast, indicated by the black line.



Fig 7. Relatively non-metamorphosed Kings Sequence protoliths.  
a) Quartz pebble conglomerate.  
b) Turbidite sequence, showing fining of sediment size from bottom right to upper left of photo.



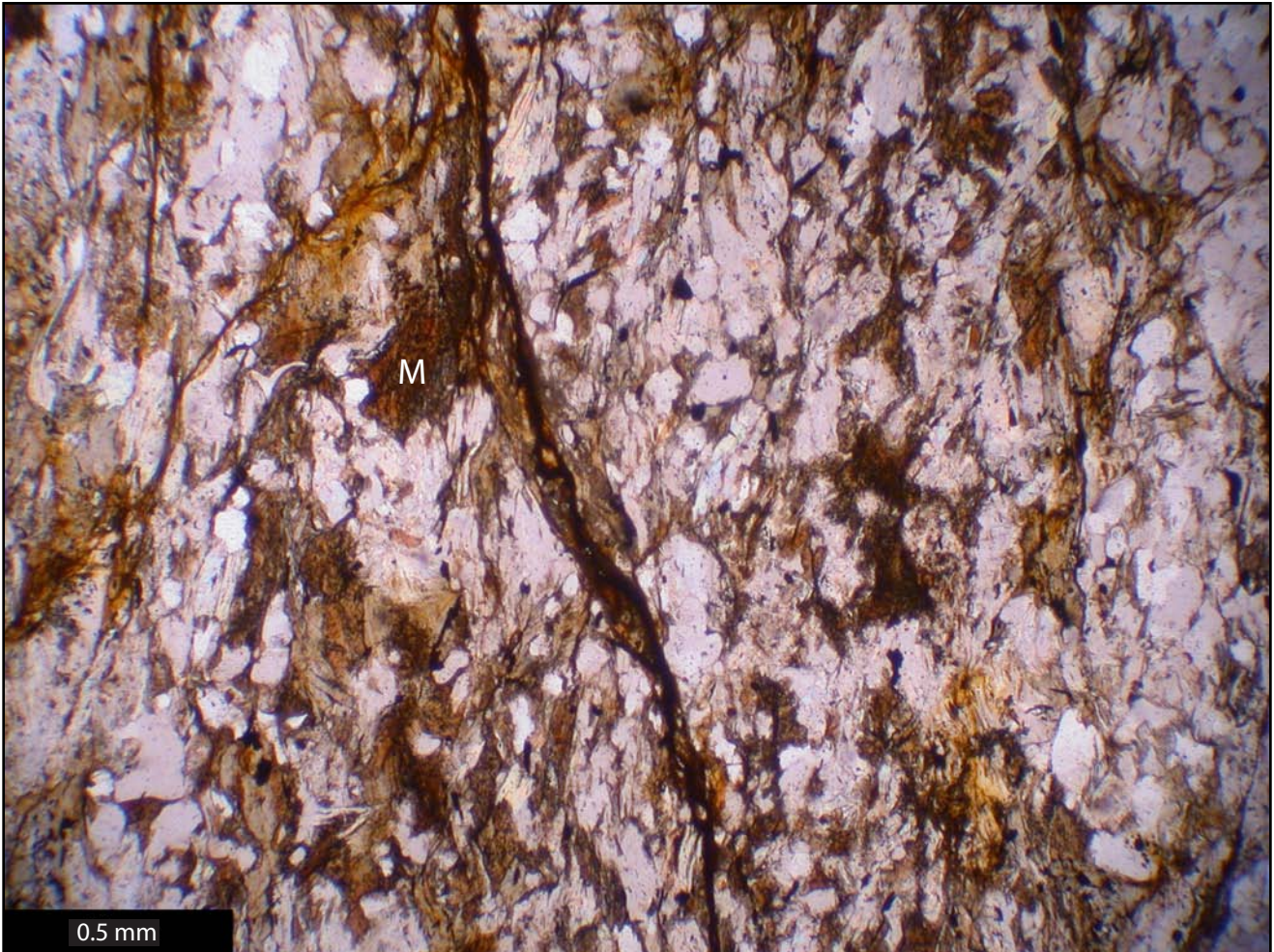
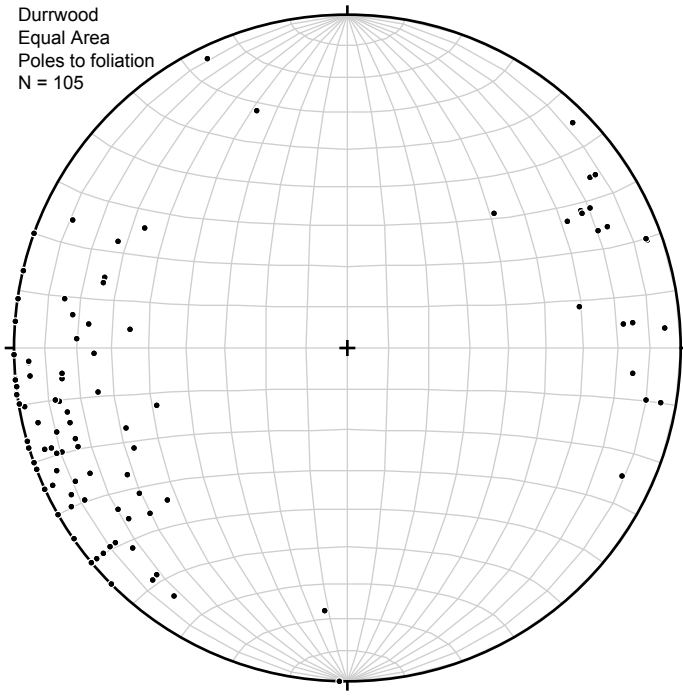
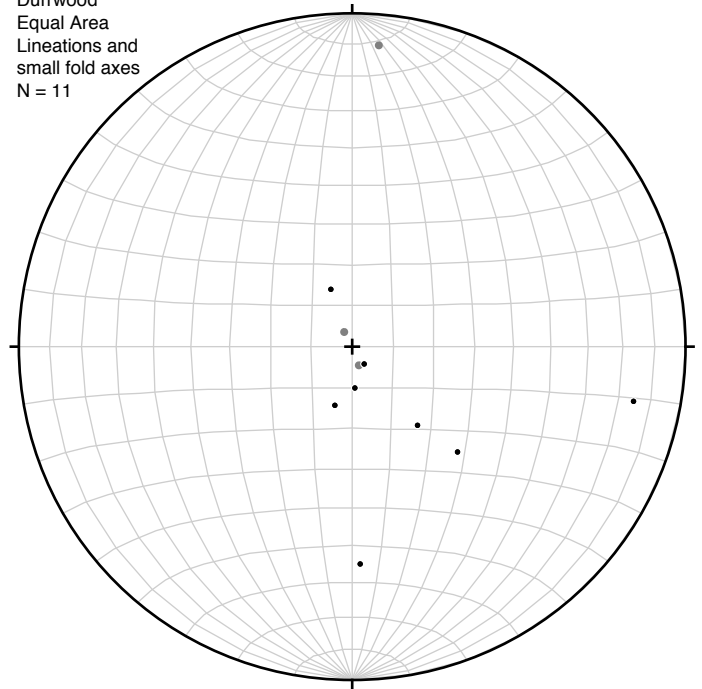


Fig 8. Anastomosing brittle-ductile shears of sample D11. Ductile shearing is defined by aligned micas (M), while through-going cracks form the brittle shears. View is plane polarized light.

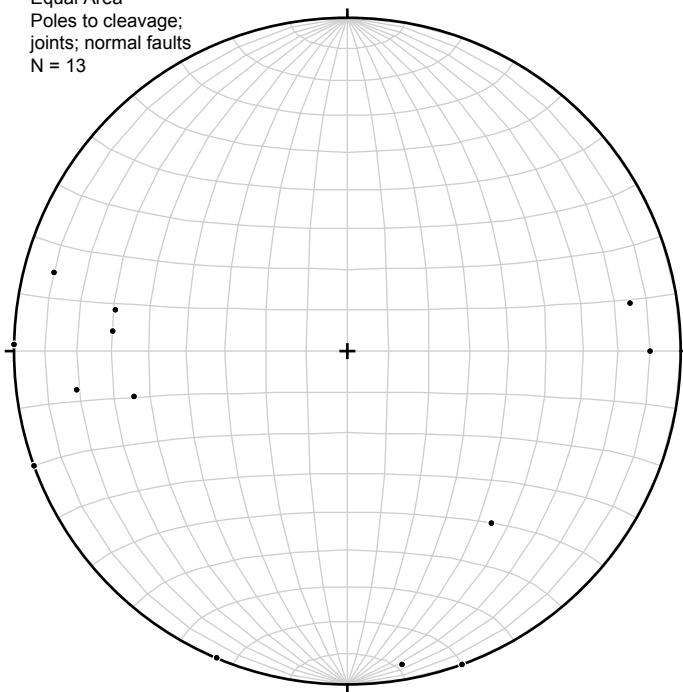
Durrwood  
Equal Area  
Poles to foliation  
N = 105



Durrwood  
Equal Area  
Lineations and  
small fold axes  
N = 11



Durrwood  
Equal Area  
Poles to cleavage;  
joints; normal faults  
N = 13



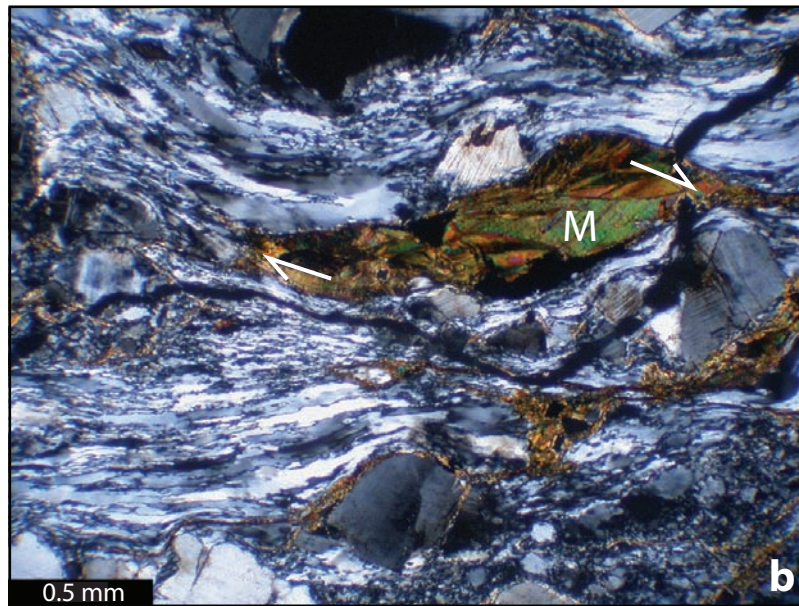
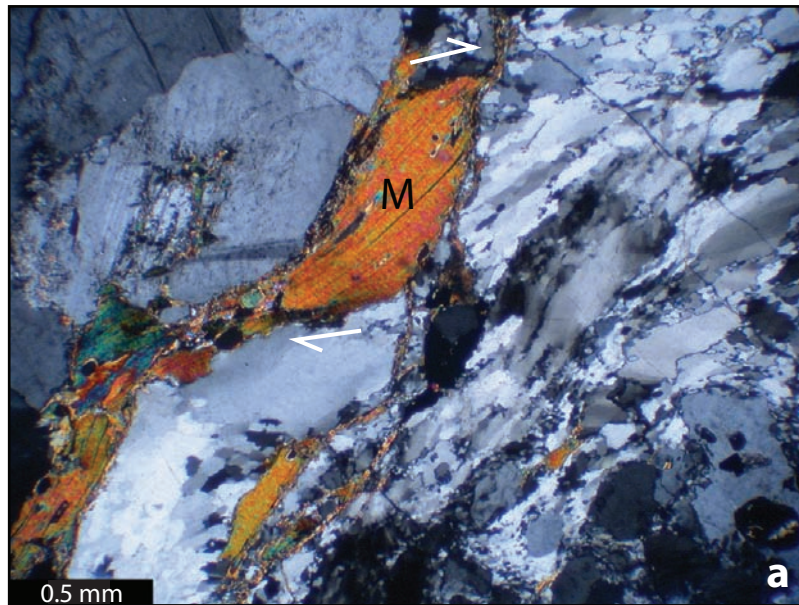


Fig 10. Biotite mica (M) "fish" indicating dextral ductile shear in samples a) D4 and b) D6. Arrows indicate sense of shear.



Fig 11. S-C granite mylonite. S-planes, or planes of flattening, are defined by elongate feldspar. C-planes, or planes of slip, are defined by aligned mica.

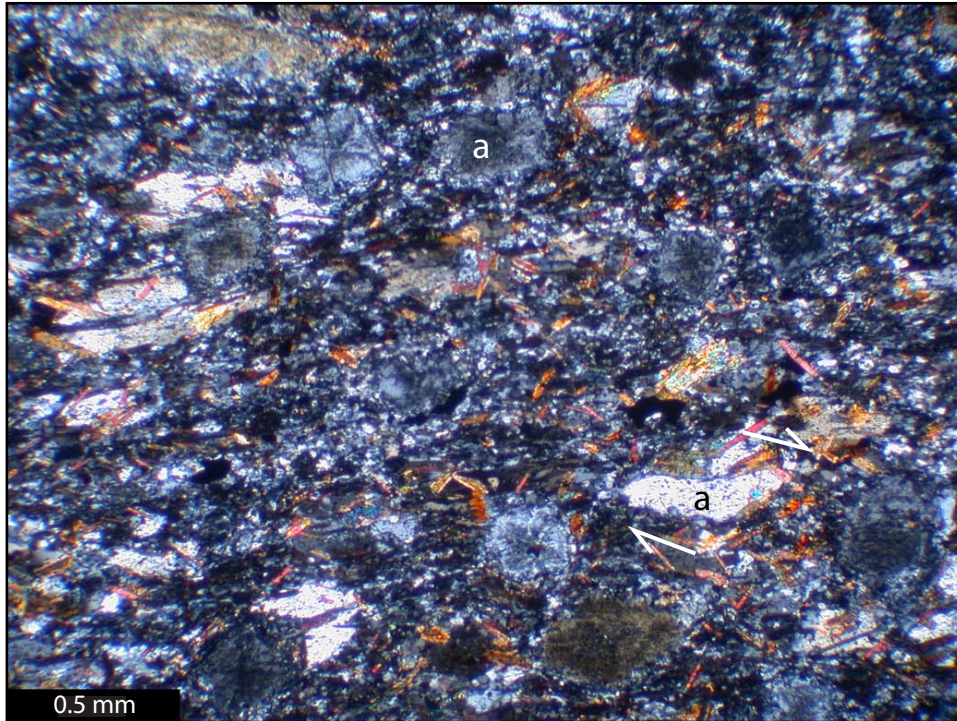


Fig 12. Andalusite schist, sample D16. The presence of opaque mineral inclusions in andalusite (a) indicates greenschist to lower amphibolite facies metamorphic grade. Some andalusite grains show rotation and growth in a dextral shear regime, as indicated by the arrows.

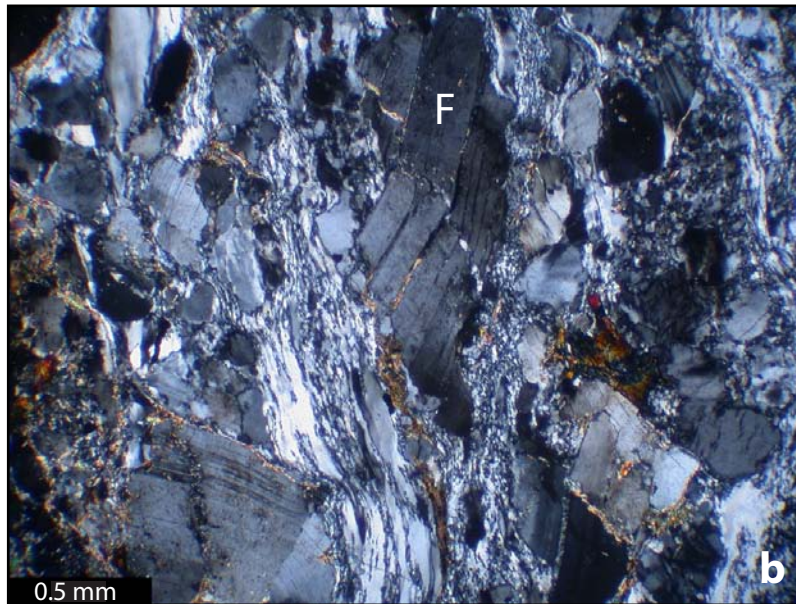
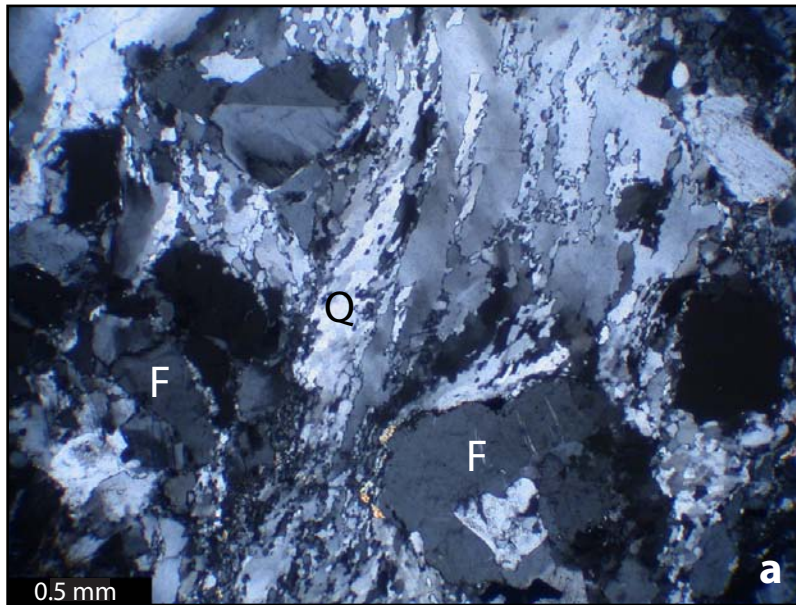
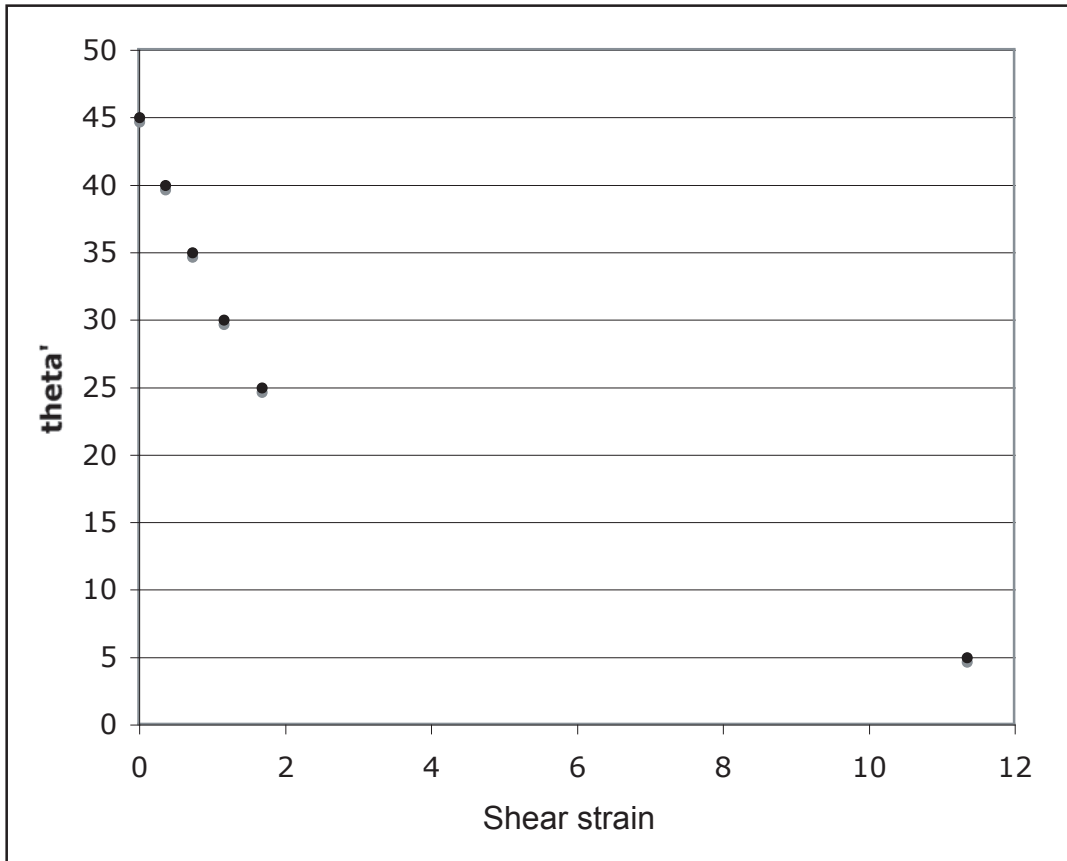
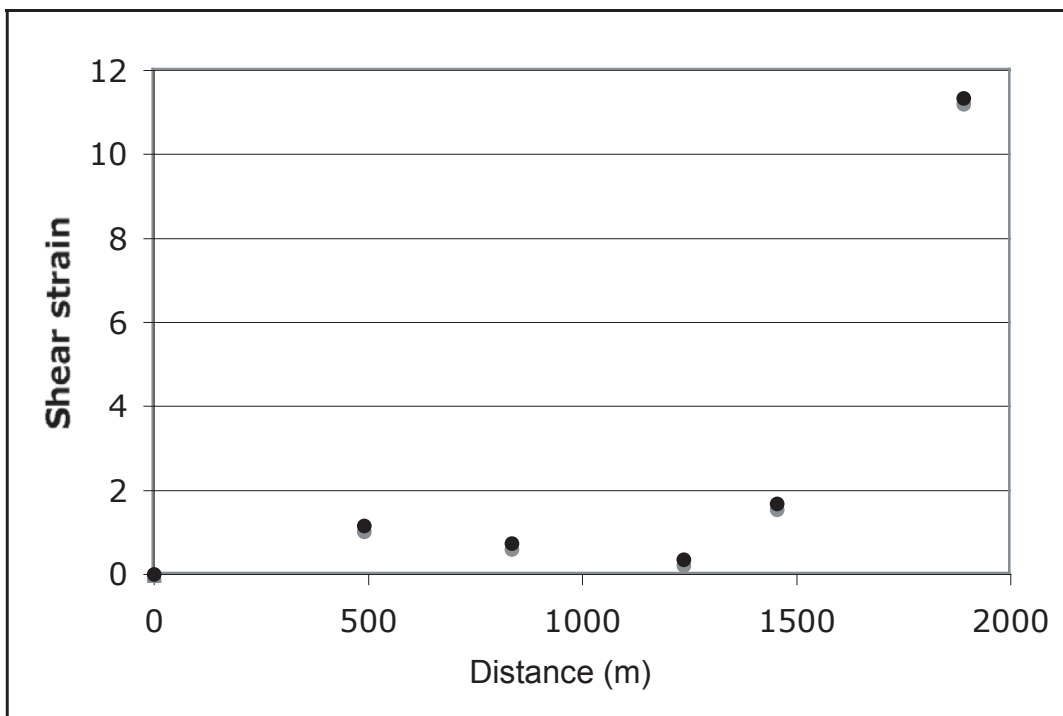
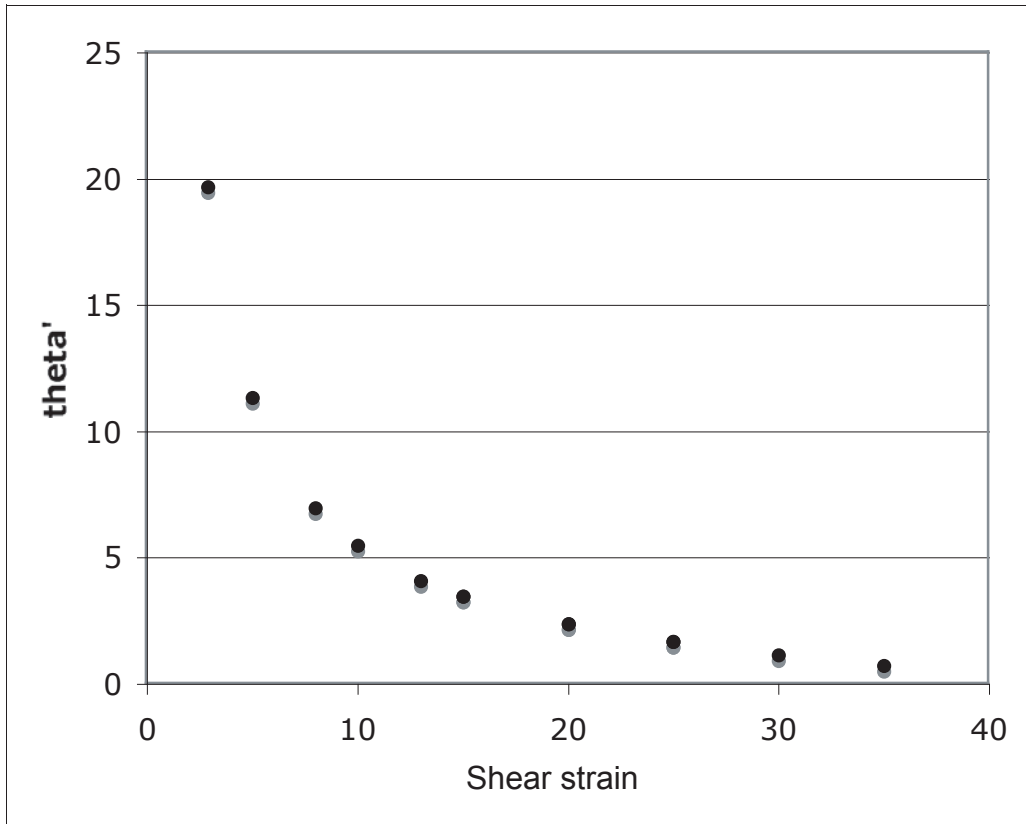
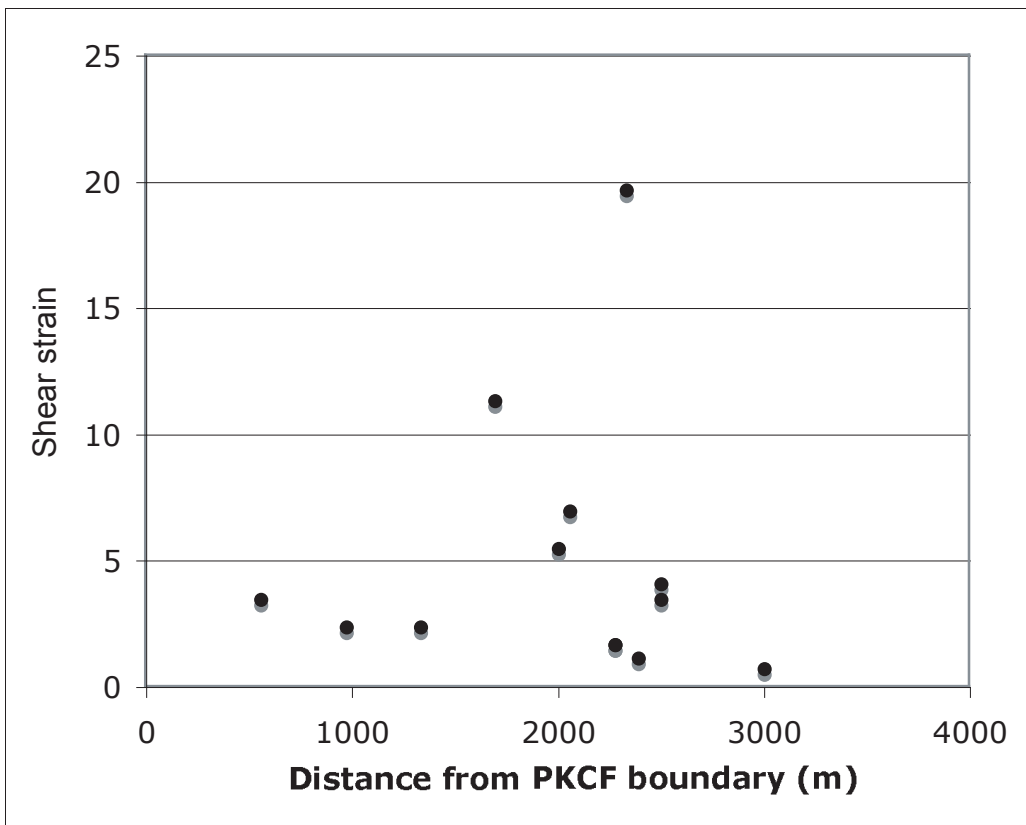


Fig 13. Granite, showing a) ductile flow of quartz (Q) in contrast with brittle deformation of feldspar (F), indicating deformation T of 300 - 400° C in sample D5, and b) "book-shelf" microfracturing of feldspar (F), indicating deformation T ~ 400° C in sample D6.

**A.****B.**

**A.****B.**

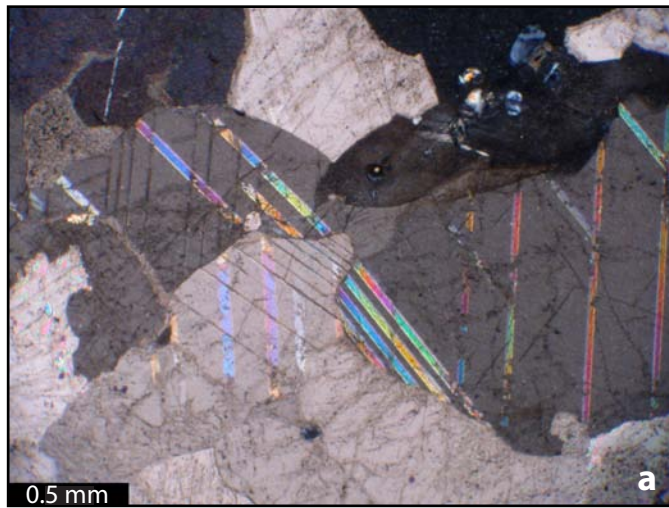
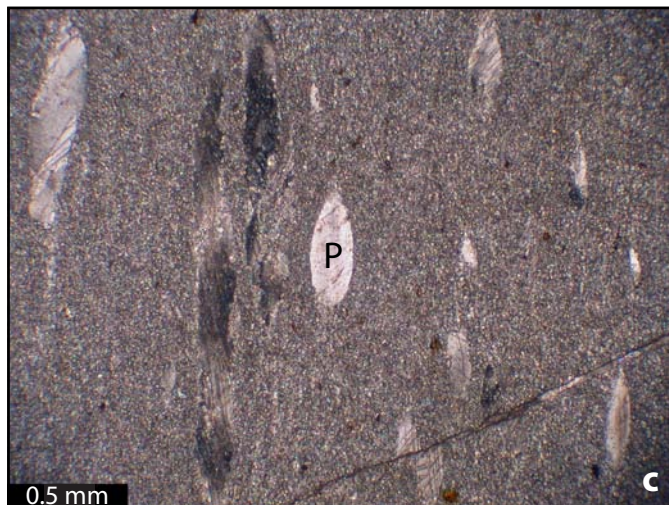
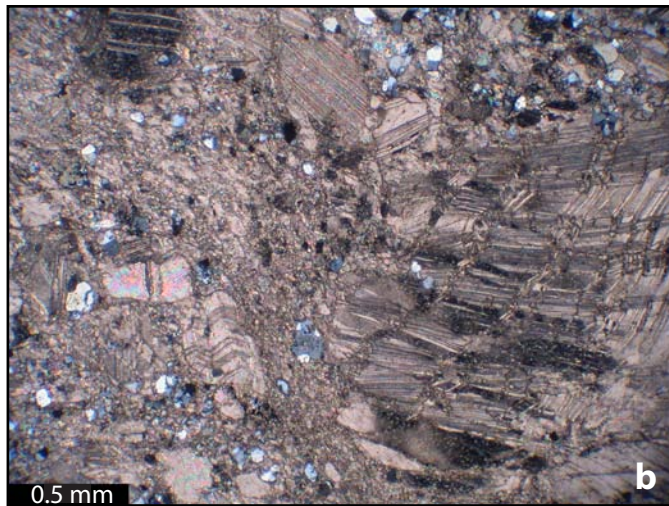


Fig 16. Marble samples, showing progressive stages in deformation. All sections are pure calcite, taken in cross polarized light. a) Annelaed fabric with thick twin lamellae indicating deformation T of 200 - 300° C. b) Complex twinning and kinking of calcite grains and grains size reduction in a marble protomylonite. c) High-grade marble mylonite has very small calcite grains with larger, stretched calcite "porphyroclasts" (P).



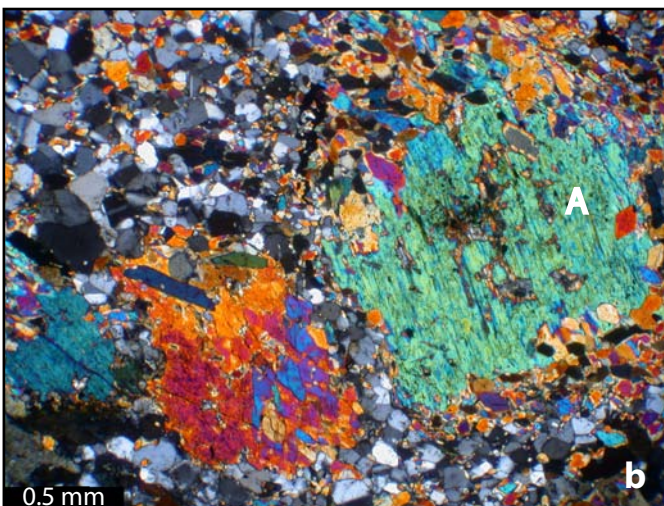
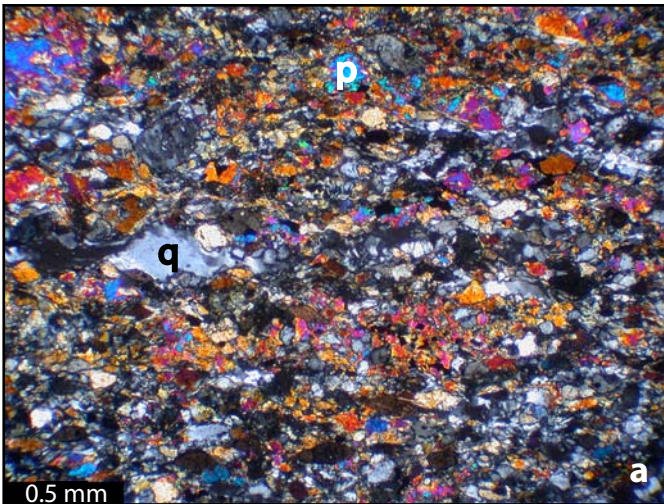


Fig 17. Calcsilicate . a) Fine-grained rock from a lens within the eastern granite, showing ductilely deformed quartz (q) and brittlely deformed (highly birefringent) pyroxene (p). b) Amphibole porphyroblast (A) is deforming brittlely as it rolls clockwise. The continuity of the grain is seen in plane polarized light (top photo), while its broken edges are seen in cross-polarized light (bottom photo). Arrow indicates direction of shear is clockwise, or right-lateral. Quartz is not deformed in this sample.

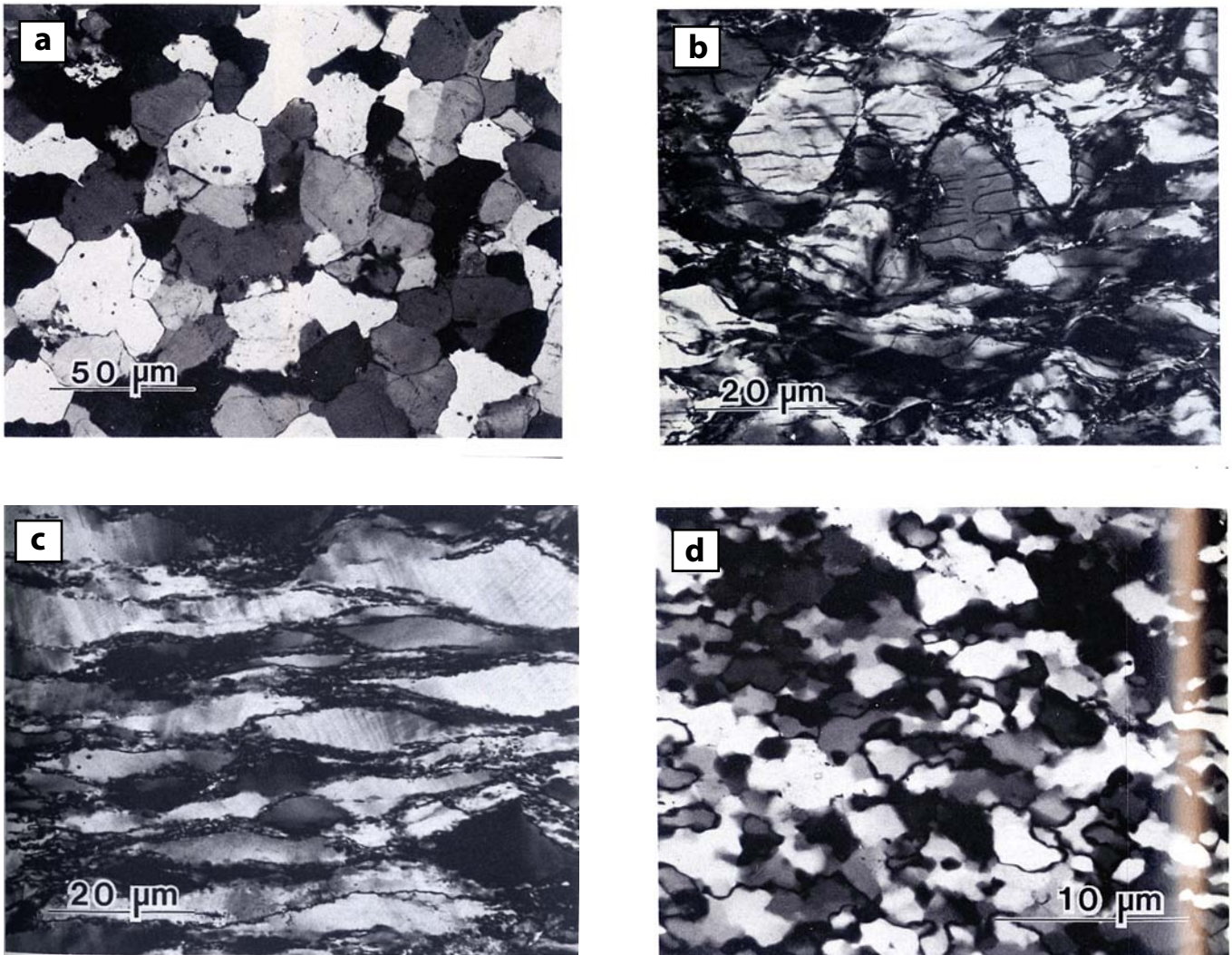


Fig 18. Quartz dislocation creep regimes of Hirth and Tullis (1992). a) Non-deformed start sample, showing sharp grain boundaries, no preferred orientation of grains, and no undulatory extinction. b) Regime 1, deformed at 700° C and  $10^{-6} \text{ s}^{-1}$ , shows heterogeneously flattened grains and patchy undulatory extinction. (Horizontal cracks arose during unloading.) c) Regime 2, deformed at 800° C and  $10^{-6} \text{ s}^{-1}$ , shows homogeneously flattened grains with sweeping undulatory extinction. d) In regime 3, deformed at 900° C and  $10^{-6} \text{ s}^{-1}$ , 100% recrystallization has rid the grains of dislocations.

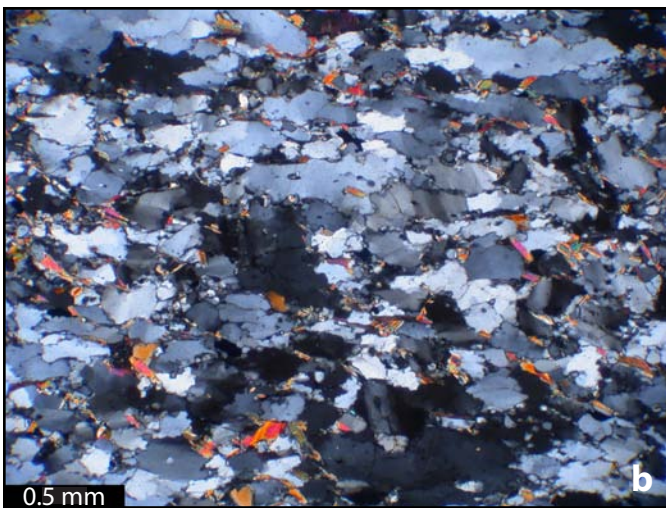
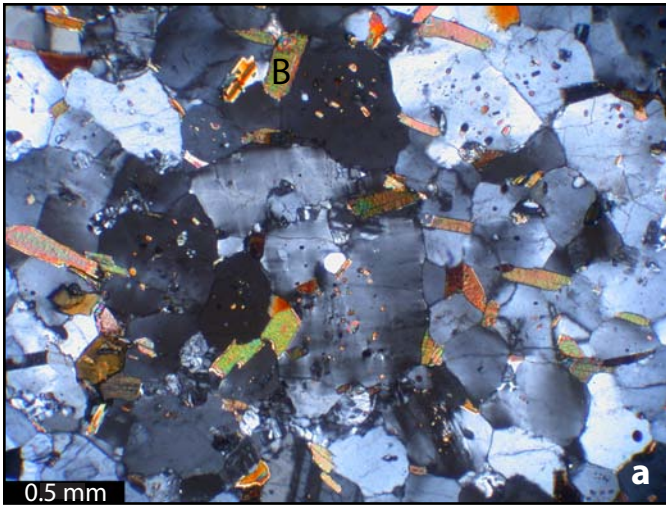


Fig 19. Quartzite from the northernmost tip of the pendant. a) Relatively coarse quartz grains (shades of grey) are virtually strain-free, showing only patchy undulatory extinction. Biotite (B) shows no preferred orientation. Sample D31. b) Finer-grained quartz is ductilely deformed in regime 1 of Hirth and Tullis (1992), as seen by heterogeneous flattening and patchy undulatory extinction. Sample D30.

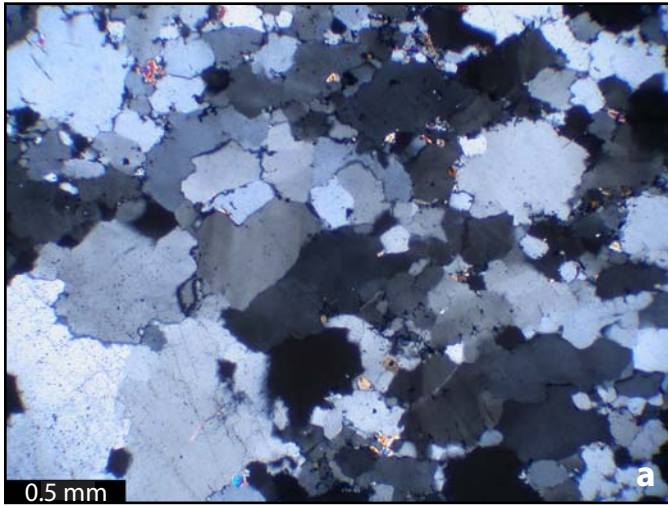
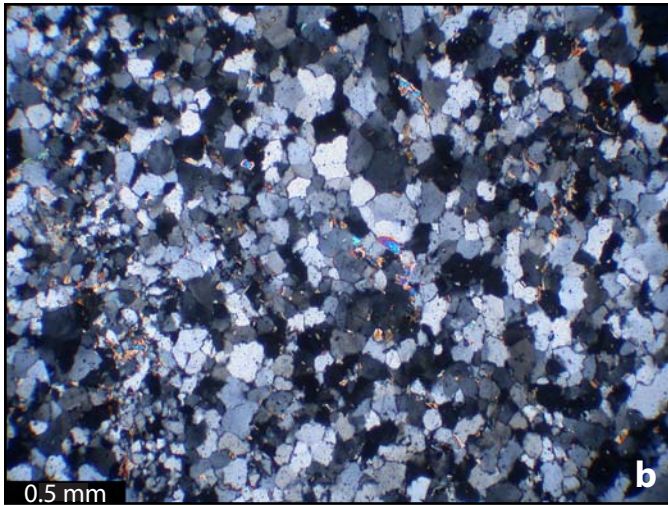


Fig 20. Quartzite from the northern half of the pendant. Both samples are composed primarily of quartz. a) Sample D35, from the western side of this section, shows marginal patchy extinction and grain flattening, indicating incipient regime 1 deformation. b) Grain boundaries from sample D38, closer to the main trace of the PKCF, are sharp, indicating no strain. Quartz in this sample also has little to no undulatory extinction.



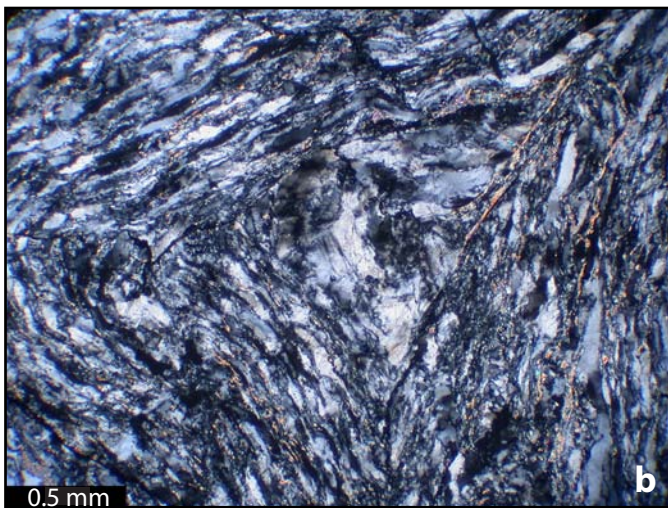
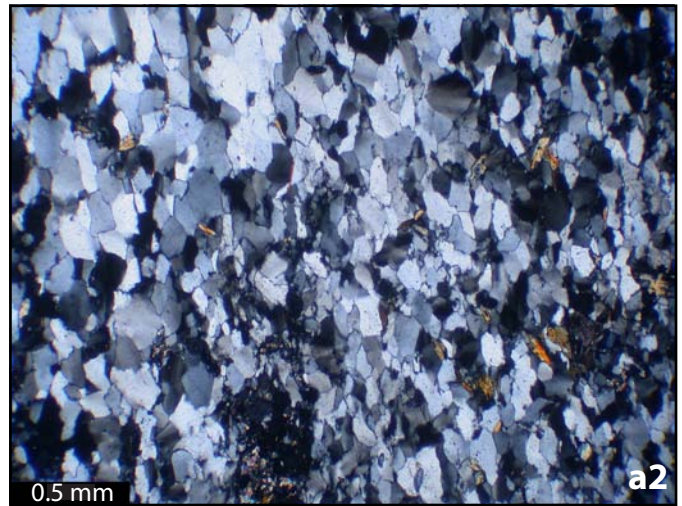
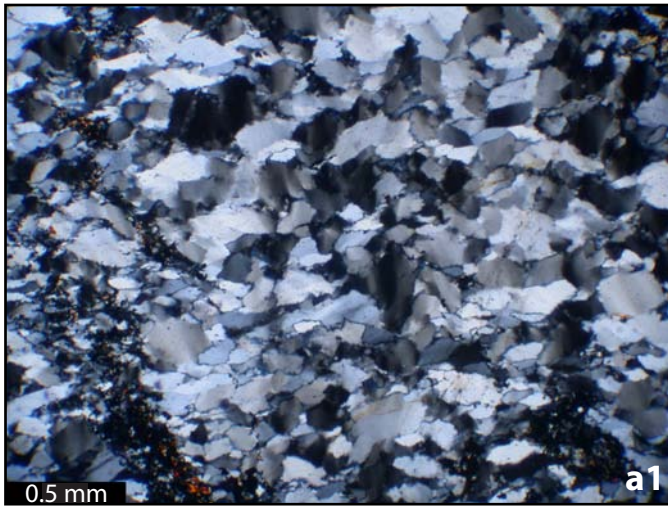


Fig 21. Quartzite from the southern half of the pendant. All samples shown are composed primarily of quartz, and are cut perpendicular to foliation. a) Quartz grains in samples D41 and D42 show heterogeneous flattening and patchy undulatory extinction of regime 1. b) Quartz grains in sample D39, from the eastern-most edge of the pendant in this segment, show the heterogeneous flattening and sweeping undulatory extinction of regime 2. This is the highest-grade quartz mylonite from the pendant in the Durrwood Creek area.

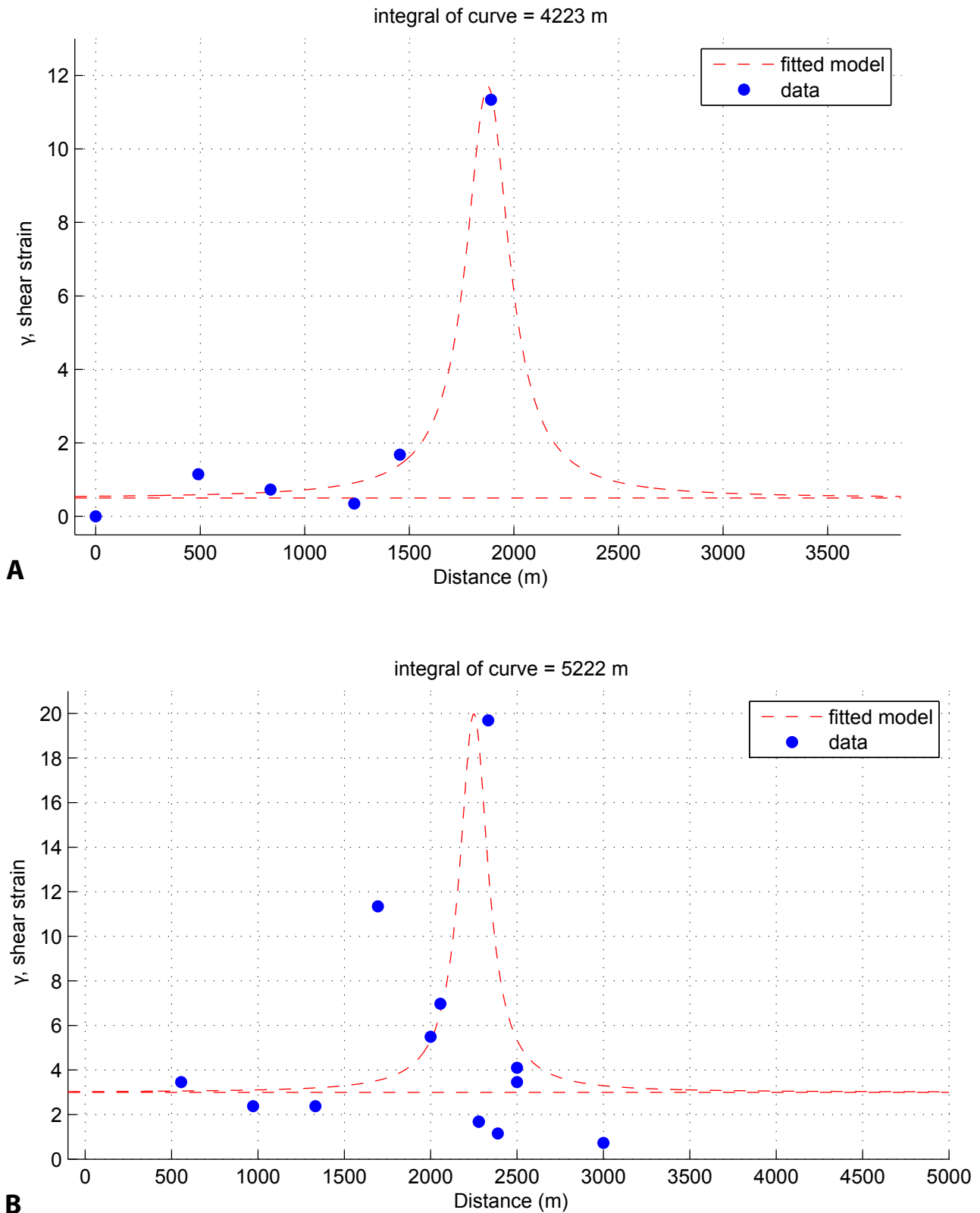


Fig 22. Curves fitted to calculations of shear strain (y-axis) as a function of distance (x-axis) across the width of the PKCF. The area under the curve represents total displacement along the shear zone. A) Shear strain measured from angles between S- and C-surfaces of granite mylonites. Displacement = 4.2 km. B) Shear strain calculated from angles between foliation (in both metamorphic pendant rocks and granite mylonite) and an average strike of the PKCF of N05E. Displacement = 5.2 km.

<b>Table 1. Durrwood Creek Map Area Samples</b>				
<b>Study ID</b>	<b>Field ID</b>	<b>UTM easting</b>	<b>UTM northing</b>	<b>Description</b>
<b>Granodiorite</b>				
D1	ESN48	368260.92	3995265.03	Kne, Granodiorite of the Needles member of the Needles intrusive suite, ca. 96.4 Ma. Generally unstrained, though biotite is slightly kinked. Myrmekitic texture indicates T ~600° C.
D2	86SS21	367892.55	3986733.09	Kpm, Granodiorite of Peppermint Meadow member of the Needles intrusive suite, ca. 97.4 Ma. Completely strain free.
<b>Granite</b>				
D3	ESN2	369189.78	3991132.16	Granitic member of Kne. Mildly deformed, some kinked feldspar.
D4	ESN1	369723.30	3991292.03	Kcr, Granite of Castle Rock member of the Domelands intrusive suite, ca. 89 Ma. Medium-strain mylonite, with dextral sense of shear indicated by mica "fish". Quartz is deformed by BLG and SGR, but feldspar deformation is dominated by brittle fracture and cataclastic flow, suggesting T < 400° C.
D5	ESN9d	370440.32	3991145.04	Kcr. Medium-strain mylonite, with ductile flow of quartz around brittley deformed feldspar, T < 400° C.
D6	ESN20	369379.40	3989836.46	Kcr. Higher-grade mylonite, with chains of stepping mica "fish" and quartz highly deformed by BLG and SGR. Feldspar exhibits "bookshelf" microfracturing, indicating T ~400° C.
D7	86SS13	369019.94	3984534.81	Kcr. Low-strain protomylonite. Quartz is deformed, but only by BLG.
D8	96SS7	368729.03	3983546.64	Kcr. Medium-strain mylonite, with quartz deformation by BLG and SGR. Brittley deformed feldspar, T < 400° C.
<b>Diamictite</b>				
D9	ESN4	368914.28	3991133.54	Low - medium strain. Strong PO of biotite visible in plain polarized light, mild straining of quartz seen under crossed polars.
D10	ESN25	369009.46	3989150.51	High-strain, high-grade conditions evident by strong PO of quartz, mica, and sillimanite. Elongated quartz defines the S-planes, and aligned mica defines the C-planes of this mylonite. Clasts of larger-grained quartzite clasts are stretched and rotated as $\delta$ -type porphyroclasts.

<b>Phyllite</b>				
D11	ESN6	368669.28	3991081.96	Some porphyroblasts of fractured amphibole, and presence of anastomosing brittle-ductile shears.
D12	ESN15	368957.41	3990576.33	Moderate PO in micas; anastomosing brittle-ductile shears.
D13	86SS23	368573.29	3986391.37	Weak PO in biotite, forming incipient crenulation cleavage, but overall low strain.
D14	ESN38a	368574.47	3986317.46	Quartz is strain-free, but mica is reduced to very fine grains.
D15	96SS6	368645.78	3983818.30	Angular quartz grains with no internal strain.
<b>Andalusite schist</b>				
D16	040619-2	368038.87	3991190.04	Medium strain, with strong PO of mica and andalusite grains. (+) andalusite growing poorly at Al-poor sites (such as opaque-rich layers) indicates greenschist/lower amphibolite facies conditions.
D17	ESN17	368795.68	3990477.80	Medium strain, with rims of andalusite porphyroblasts altering to muscovite. Mica trails give conflicting, but mostly dextral sense of shear.
<b>Calcsilicate</b>				
D18	ESN50	368256.52	3994723.04	Low strain, localized in quartz. Orthopyroxene, amphibole, and feldspar are strain-free.
D19	ESN9a	370437.14	3991147.03	Medium strain localized in quartz, which flows around brittlely deforming sphene and pyroxene.
D20	040619-1	367993.47	3991252.57	Medium strain, indicated by large amphibole crystals reduced to many new, small grains via dynamic recrystallization.
D21	040620-2	367890.14	3991230.09	Strain free, fine grained, orthopyroxene- and amphibole-rich.
D22	86SS26	368290.77	3982465.69	Low strain, with quartz deforming via BLG, and finely recrystallized mica. Late-stage brittle-ductile shears are filled with mica.
<b>Marble</b>				
D23	ESN28	369115.77	3991766.34	Recrystallized but pervasively twinned, with Type II twins indicated $T = 200^{\circ} - 300^{\circ} \text{C}$ .
D24	ESN42	368747.35	3986635.34	High strain, very fine-grained calcite grains with larger strained "porphyroclasts". Lamellae twins are bent, indicating dextral shear. Late-stage brittle fracture and coarser-grained vein fill.
D25	86SS22	368129.33	3986641.61	Recrystallized, large grains, but thick (Type II) twin lamellae.
D26	ESN38b	368589.95	3986310.27	Low- to medium-strain, with mix of large and small grains. Tabular, thick Type II twins; twin width $\sim 3 \text{um}$ indicates shear strain $\sim 0.4$ .

D27	86SS24	368737.42	3986254.15	Just like D26
D28	86SS25	368823.52	3985858.62	Medium strain, intermediate between D23 and D24. Shapes of calcite "porphyroclasts" indicate dextral shear.
D29	96SS2A	368159.43	3984033.00	Low to medium strain, complex twinning and kinking of large calcite grains.
<b>Quartzite</b>				
D30	040617-2	368498.87	3994868.45	Strong PO of biotite. Elongated quartz grains with subgrains and irregular grain boundaries indicate grain boundary migration under medium strain.
D31	040617-3	368547.34	3994855.23	Low strain, with annealed texture, larger grain size than D30, and weak PO of biotite.
D32	040620-1	367899.60	3991259.60	Annealed texture, with (+) sillimanite and garnet indicating high-T, probably lower amphibolite facies conditions.
D33	040620-3	367798.25	3991145.03	Annealed texture.
D34	040619-3	368156.12	3990883.83	Low strain, almost pure quartzite with large grains and small neoblasts along grain margins indicating shear strain < 1.
D35	040619-4	368308.75	3990738.55	Same as D34.
D36	040619-5	368252.11	3990655.92	Strong PO of biotite, and some grain boundary migration indicate some strain, but the presence of an unstrained quartz vein probably post-dates deformation.
D37	ESN5	368656.26	3991251.13	Strong PO of mica, fine-grained, with remnants of finer-grained patches that seem to have concentrated stress.
D38	ESN16	368936.97	3990371.84	
D39	ESN22	369143.31	3989405.18	Folded pure quartzite, with quartz grains stretched into a tight fold, and mica reduced to very fine grains, suggesting high strain.
D40	ESN39	368661.84	3986276.56	Strong SPO indicates high strain.
D41	96SS1B+1A	367879.01	3983612.37	Highly strained, strong PO, with SGR and BLG.
D42	96SS3A	367795.76	3983130.39	Medium strain indicated by moderate PO of quartz and mica, stretched quartz grains, and more BLG than SGR.
(S)PO = (shape) preferred orientation				
BLG = bulging recrystallization, Regime 1 of Hirth and Tullis (1992).				
SGR = Subgrain Rotation recrystallization, Regime 2 of Hirth and Tullis (1992).				